AGU PUBLICATIONS

JGR

Journal of Geophysical Research: Solid Earth

RESEARCH ARTICLE
10.1002/2014JB011150

Key Points:
- Three-dimensional numerical modeling of western Mediterranean subduction evolution since 35 Ma
- Modeled subduction evolution distinguishes between disparate tectonic scenarios
- Preferred model matches observed slab morphology and key temporal constraints

Supporting Information:
- Readme
- Figures S1–S4

Correspondence to:
M. V. Chertova,
m.v.chertova@uu.nl

Citation:
Chertova, M. V., W. Spakman, T. Geenen, A. P. van den Berg, and D. J. J. van Hinsbergen (2014), Underpinning tectonic reconstructions of the western Mediterranean region with dynamic slab evolution from 3-D numerical modeling, *J. Geophys. Res. Solid Earth*, *119*, doi:10.1002/2014JB011150.

Received 26 MAR 2014
Accepted 12 JUN 2014
Accepted article online 18 JUN 2014

Underpinning tectonic reconstructions of the western Mediterranean region with dynamic slab evolution from 3-D numerical modeling

M. V. Chertova[1], W. Spakman[1,2], T. Geenen[3], A. P. van den Berg[1], and D. J. J. van Hinsbergen[1]

[1]Department of Earth Sciences, Utrecht University, Utrecht, Netherlands, [2]Centre of Earth Evolution and Dynamics, University of Oslo, Oslo, Norway, [3]SURFsara, Amsterdam, Netherlands

Abstract No consensus exists on the tectonic evolution of the western Mediterranean since ~35 Ma. Three disparate tectonic evolution scenarios are identified, each portraying slab rollback as the driving mechanism but with rollback starting from strongly different subduction geometries. As a critical test for the validity of each tectonic scenario we employ thermomechanical modeling of the 3-D subduction evolution. From each tectonic scenario we configure an initial condition for numerical modeling that mimics the perceived subduction geometry at ~35 Ma. We seek to optimize the fit between observed and predicted slab morphology by varying the nonlinear viscoplastic rheology for mantle, slab, and continental margins. From a wide range of experiments we conclude that a tectonic scenario that starts from NW dipping subduction confined to the Balearic margin at ~35 Ma is successful in predicting present-day slab morphology. The other two scenarios (initial subduction from Gibraltar to the Baleares and initial subduction under the African margin) lead to mantle structure much different from what is tomographically imaged. The preferred model predicts slab rotation by more than 180°, east-west lithosphere tearing along the north African margin and a resulting steep east dipping slab under the Gibraltar Strait. The preferred subduction model also meets the first-order temporal constraints corresponding to Mid-Miocene (~16 Ma) thrusting of the Kabylides onto the African margin and nearly stalled subduction under the Rif-Gibraltar-Betic arc since the Tortonian (~8 Ma). Our modeling also provides constraints on the rheological properties of the mantle and slab, and of continental margins in the region.

1. Introduction

For the western Mediterranean region (Figure 1), distinctly different tectonic reconstructions exist for the past ~35 My, which all appear to be based on broadly similar geological and plate kinematic constraints [e.g., *Rosenbaum et al*., 2002; *Faccenna et al*., 2001a, 2001b, 2004; *Jolivet et al*., 2009; *Schettino and Turco*, 2006; *Handy et al*., 2010; *Carminati et al*., 2012; *Vergés and Fernàndez*, 2012; *van Hinsbergen et al*., 2014]. Despite the large consensus that subduction rollback since ~35 Ma is regarded as the geodynamic process driving tectonic change, there is significant disagreement on its spatial-temporal evolution and how this couples to tectonic evolution. Rollback is either portrayed as originating from a long N-NW dipping subduction zone stretching from Gibraltar in the west to the Baleares in the NE [e.g., *Dercourt et al*., 1986; *Faccenna et al*., 2004; *Schettino and Turco*, 2006; *Handy et al*., 2010; *Carminati et al*., 2012], or from a laterally restricted NW dipping slab confined to the Baleares margin [e.g., *Rosenbaum et al*., 2002; *Spakman and Wortel*, 2004; *Frizon de Lamotte et al*., 2009; *van Hinsbergen et al*., 2014], or from a SE dipping subduction under the north-African margin [*Vergés and Fernàndez*, 2012] (Figure 2). These three disparate tectonic evolution scenarios illustrate the current lack of convergence toward a single tectonic evolution model for the western Mediterranean.

Although collecting more geological and geophysical data may perhaps provide a resolution, we followed the, as yet, unexplored avenue of designing and applying quantitative tests for the various proposed geodynamic rollback hypotheses. The most crucial test is whether 35 My of subduction evolution, as qualitatively portrayed in each tectonic reconstruction, can predict the position and 3-D morphology of tomographically imaged slabs in the upper mantle of the region. To investigate this we employed 3-D thermomechanical subduction modeling starting from an initial configuration defined from each tectonic reconstruction. In this "forward" approach we experimented with different initial settings for the rheology of the mantle, lithosphere, and continental margins and their geometry as a strategy to optimize the fit between predicted and observed slab position and morphology. This is different from "inverse" approaches in which

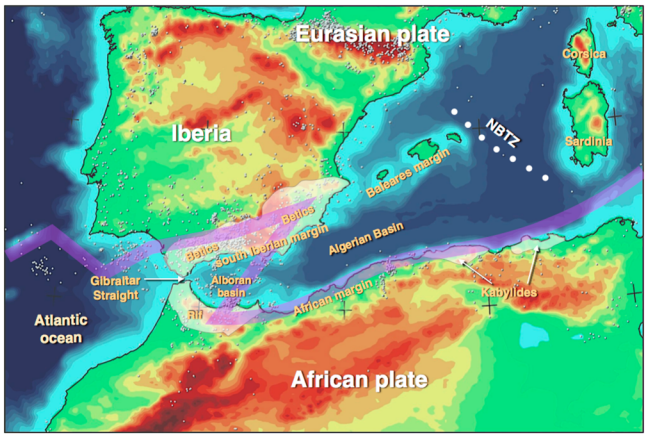

Figure 1. Map of the westernmost Mediterranean region with the main geographic names and some tectonic features used in the paper. NBTZ-North Balearic Transform Fault zone. The transparent purple line depicts the diffuse plate boundary between the African and Eurasian plate in the region [after *Gutscher et al*., 2012].

the tomographic model is input to reconstruct the initial condition, i.e., the past [e.g., *Liu and Gurnis*, 2008; *Ismail-Zadeh et al*., 2012; *Spasojević et al*., 2009]. Here we specifically conformed to the 3-D geometry of the subduction zone at ~35 Ma as portrayed in, or derived from, a tectonic reconstruction to define the initial condition for 3-D modeling and next predict the future. Our results show a strong difference in subduction evolution between the different tectonic reconstructions and a strong dependence on assumed rheology. However, a suite of different experiments, in which also initial conditions are varied within the limits posed by a particular reconstruction, led to a clear and positive outcome.

The generic research aim we pursue here is to make a significant step forward from kinematics-based tectonic reconstructions toward dynamics-based reconstructions in which the role of deep driving processes that underpin regional tectonic evolution is quantitatively assessed and incorporated. The initial step we make is quantitative testing, through 3-D numerical modeling, of the qualitative concepts of the driving geodynamic processes that have been proposed to underpin the kinematic reconstruction of tectonic evolution. This proves to be a very powerful strategy for constraining the tectonic evolution of the western Mediterranean.

2. Modern Mantle Structure From Seismic Tomography: The Rif-Gibraltar-Betic Slab

Early tomographic observation of a positive seismic velocity anomaly across the upper mantle of the western Mediterranean region led to the first interpretations of deep subduction [*Spakman*, 1986; *Blanco and Spakman*, 1993]. Since the late 1990s, improved tomographic models all exhibit a volume with positive *P* wave speed anomalies, which extends from under the Rif-Gibraltar region curving to the NE and E to under the eastern Betics (Figure 3)[*Bijwaard et al*., 1998; *Calvert et al*., 2000; *Gutscher et al*., 2002; *Piromallo and Morelli*, 2003; *Spakman and Wortel*, 2004; *Bezada et al*., 2013; *Palomeras et al*., 2014]. A breakthrough interpretation was made by *Gutscher et al*. [2002] who explained marine geophysical observations of an active fore arc west of the Gibraltar Strait with the existence of a continuous east dipping

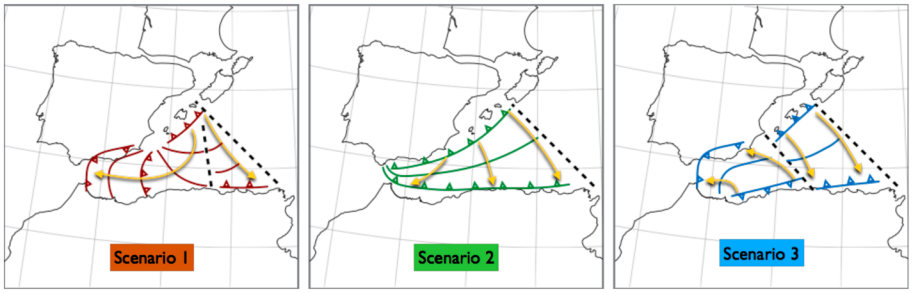

Figure 2. An illustration of rollback as portrayed in the three different reconstruction scenarios shown in the paleogeography at ~35 Ma [*van Hinsbergen et al*., 2014]: Scenario 1 starts from an initial short subduction zone near the Baleares [e.g., *Rosenbaum et al*., 2002; *Spakman and Wortel*, 2004; *van Hinsbergen et al*., 2014]; Scenario 2 involves a long initial trench along the entire Gibraltar-Baleares margin [e.g., *Gueguen et al*., 1998; *Faccenna et al*., 2004; *Jolivet et al*., 2009]; and Scenario 3 starts from a S-SE dipping initial subduction zone under African margin [*Vergés and Fernàndez*, 2012]. Dashed lines represent proposed transform fault regions. The triangular zone between the transform zones of Scenario 1 depicts the lithosphere that rolls back toward the east Kabylides [*Spakman and Wortel*, 2004]. Not displayed is the more eastern subduction system leading to rollback to the E-SE involving the Apennines-Calabria subduction system [e.g., *Faccenna et al*., 2004; *Spakman and Wortel*, 2004]. Paleogeography at 35 Ma from *van Hinsbergen et al*. [2014].

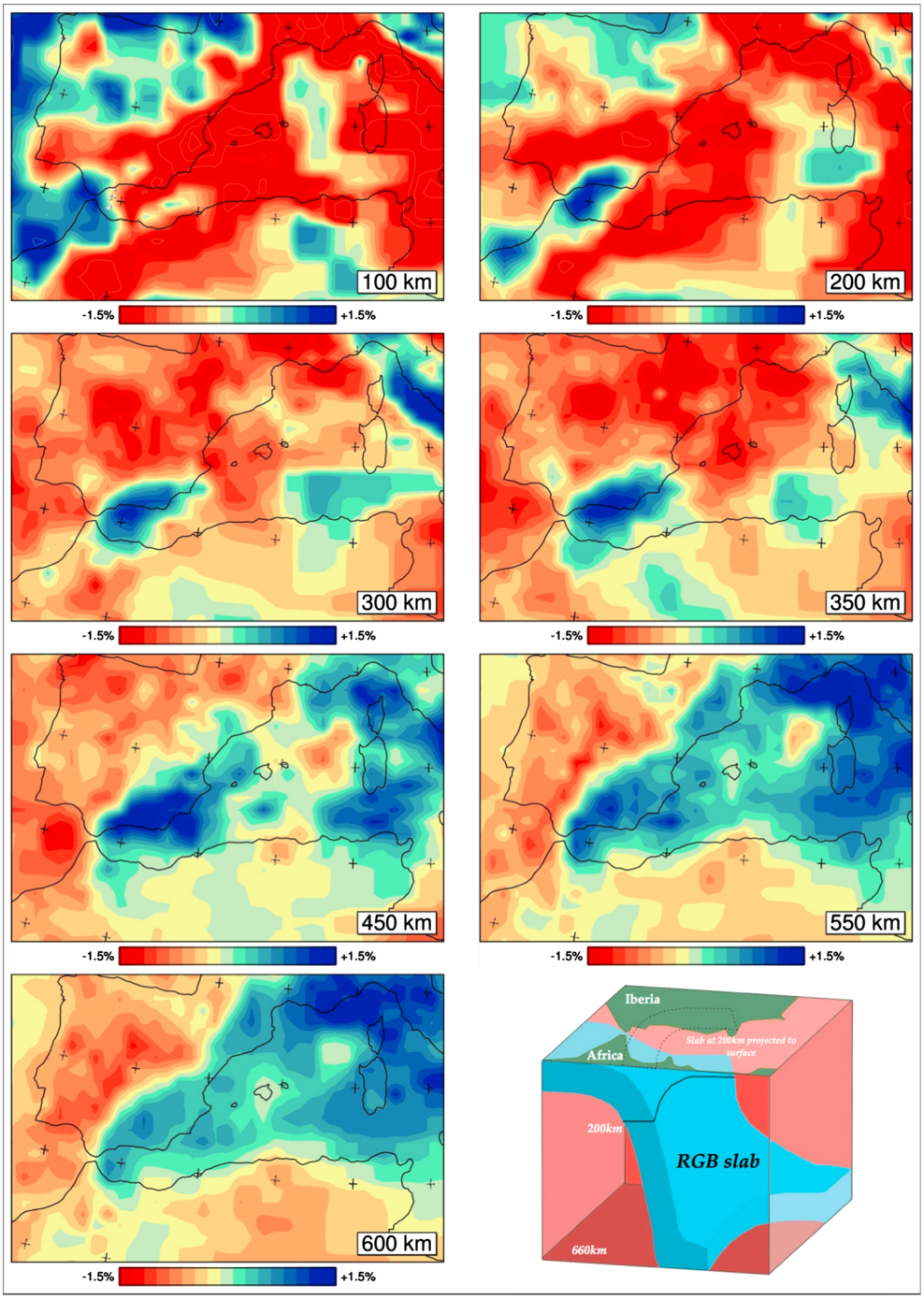

Figure 3. Mantle structure of the Western-Mediterranean region from the tomography model UU-P07 [*Amaru*, 2007]. Shown are *P* wave seismic velocity anomalies relative to the 1-D reference model ak135 of *Kennett et al.* [1995]. The blue anomaly under the Rif, Gibraltar Straight, and Betics (southern Iberia) is the blurred image of the Rif-Gibraltar-Betic (RGB) slab. The spatial resolution is presented in *van Hinsbergen et al.* [2014]. The first-order slab structure is similar to that obtained by *Bezada et al.* [2013] from tomographic analysis of an independent regional data set. A cartoon interpretation of the RGB-slab following *Spakman and Wortel* [2004] is presented at the lowest right.

slab. We refer to *Gutscher et al.* [2012] for an extensive review on present-day subduction under the Gibraltar Strait and for the evidence of the predominantly oceanic nature of the subducted lithosphere. *Spakman and Wortel* [2004] analyzed the 3-D morphology of this subducted lithosphere, which we name here the Rif-Gibraltar-Betic (RGB) slab to emphasize its lateral extent (Figure 3).

The slab image displayed in Figure 3 is from the model of *Amaru* [2007] and is of comparable morphology but of higher amplitude compared to the anomaly in the model of *Bijwaard and Spakman* [2000], which was used by *Gutscher et al*. [2002] and *Spakman and Wortel* [2004]. *Bezada et al*. [2013] recently obtained a similar tomographic image of the RGB slab from a regional tomographic analysis of a new teleseismic data set observed with a dense regional station network. Figure 3 presents the target slab morphology of which we attempt to reproduce first-order features by numerical simulation of the RGB-slab evolution. The robust features from independent tomographic studies are the steeply east dipping slab under the Gibraltar Strait and Alboran basin, and a slab morphology that extends from under the NW Rif toward the north and next curving eastward under the Betics. Most of the anomaly is found under south Iberia while in the transition zone the anomaly may also partly lie under the Algerian basin. Furthermore, under the northwest African margin, no evidence is found for subducted lithosphere, either attached or detached (*Spakman and Wortel* [2004]; *Bezada et al*. [2013]; *van Hinsbergen et al*. [2014], and spatial resolution estimates presented in these papers), whereas a detached slab is imaged below the Kabylides in northeast Algeria [*Spakman and Wortel*, 2004; *van Hinsbergen et al*., 2014]. The recent surface wave tomography model of *Palomeras et al*. [2014] corroborates the slab detachment geometry imaged under the eastern Betics (Figure 3) [*Spakman and Wortel*, 2004; *Bezada et al*., 2013] and, in addition, proposes slab continuous with the Moroccan Rif lithosphere and also slab partly attached to Iberian lithosphere under the central Betics.

3. Tectonic Reconstructions of the Western Mediterranean Region

We categorize published tectonic reconstructions into three evolution scenarios of the western Mediterranean, which we briefly introduce here in the same order as we use them for our numerical experiments. Our focus is on how subduction evolution is portrayed in these scenarios from the start of rollback at ~35 Ma and not on the geological evidence and interpretations underlying the construction of these tectonic models.

The first reconstruction scenario (S1) proposes that subduction in the western Mediterranean started from a NE-SW striking trench located southeast of the Balearic islands leading, after initial southward rollback, to a dominant phase of westward rollback of the RGB slab [e.g., *Royden*, 1993; *Lonergan and White*, 1997; *Rosenbaum et al*., 2002; *Spakman and Wortel*, 2004; *van Hinsbergen et al*., 2014]. Here we follow the analysis of *Spakman and Wortel* [2004] and *van Hinsbergen et al*. [2014] who qualitatively reconciled tectonic evolution with subduction evolution and present-day slab morphology. The initial trench was ~300 km wide measured from the North Balearic Transform Fault (NBTZ) to the southwest. Plate convergence between Africa and southern Iberia in these models is deemed insufficient to form a subduction zone and was accommodated by thrusting and Iberian margin thickening. The basic concept of trench evolution as a result of rollback is sketched in Figure 2, Scenario 1. The proposed direction of initial rollback is southward during the first 5–10 My. This is followed by rapid Early Miocene radially outgrowing rollback to the W, S, and SE. S-SE rollback of the eastern part of the slab culminates in Mid-Miocene thrusting of the Kabylides fold-thrust belt over the African margin in Algeria. Here the slab splits into two parts. The western part of the subduction zone, rotated ~100° clockwise by then into a N-S position, rolls back toward Gibraltar in the west and the south Iberian margin in the northwest. The eastern part of the slab, which underlies the eastern part of the Kabylides (Figure 1), detaches and is tomographically detected in the upper mantle below the African margin of northeast Algeria (Figure 3) [*Spakman and Wortel*, 2004; *van Hinsbergen et al*., 2014]. Our focus here is on the western part of the subduction system that at this stage was extending from the central Algerian margin to the Baleares margin. Its southern part rolled back rapidly in westward direction toward Gibraltar since Middle Miocene time accommodated by lithosphere tearing creating a subduction-transform edge propagator (STEP) fault [*Govers and Wortel*, 2005] parallel to the north African margin, which results in opening the Algerian basin by $>$500 km of E-W extension [*Mauffret et al*., 2004]. The northern part of the slab rolled back with a slower rate, likely because it subducted the southern continental margin of Iberia instead of oceanic lithosphere. This led to an additional ~80° clockwise rotation of the northern segment, culminating in an E-W, southward dipping orientation of the slab below the south Iberian margin. In all reconstructions, the slab arrives near its modern position in the Tortonian, complying with the geological evidence coming from uppermost Tortonian and Messinian sediments unconformably covering the Gibraltar trench, both onshore and offshore [*Crespo-Blanc and Campos*, 2001; *Melialdea et al*., 2004; *Chalouan et al*., 2006; *Iribarren et al*., 2007; *Ammar et al*., 2007].

The second reconstruction scenario (S2) assumes that already in the Early Oligocene an initial subduction zone of long lateral extent existed from the Baleares margin to Gibraltar (Figure 2, Scenario 2). This has been a leading

concept for more than two decades [e.g., *Dercourt et al*., 1986; *Gueguen et al*., 1998; *Wortel and Spakman*, 2000; *Faccenna et al*., 2004; *Jolivet and Faccenna*, 2000; *Jolivet et al*., 2009; *Schettino and Turco*, 2006; *Handy et al*., 2010; *Billi et al*., 2011; *Carminati et al*., 2012]. Particularly, *Faccenna et al*. [2004] coupled the tectonic evolution of the Western Mediterranean to present-day mantle structure as imaged by *Piromallo and Morelli* [2003]. In this reconstruction, the subduction process was already developed at ~35 Ma with a slab length of up to ~400 km. This maximum estimate resulted from the difference between tomographically observed slab length and the total amount of plate convergence and tectonic shortening near Gibraltar during the past ~35 My. However, the initial slab might have been shorter (at ~35 Ma) if the subducted lithosphere was weak enough to significantly stretch during subduction rollback since 35 Ma [*Faccenna et al*., 2004]. Oligocene to Middle Miocene rollback was largely southward leading to the opening of the Algerian basin in a predominant N-S direction toward Africa (Figure 2, Scenario 2) and thrusting of the Kabylides onto the African margin in the Middle Miocene. A subsequent rapid clockwise trench rotation toward present-day Gibraltar was accommodated along the Rif margin, followed by ~200 km of E-W extension of the Alboran domain.

The recent reconstruction model of *Vergés and Fernàndez* [2012] constitutes our third scenario S3. In contrast to initial subduction under the European (Iberian-Baleares) margin, as in scenarios S1 and S2, an initial Early-Middle Cenozoic subduction zone is proposed that dipped southward below the North African margin. It is tectonically broadly similar to the westward rollback phase of scenario S1 in that it invokes large-scale northwestward and westward rollback of the RGB-slab accommodated by E-W opening of the Algerian basin (Figure 2, Scenario 3). This initially south dipping subduction zone was of 400–500 km lateral extent, situated under the western Algerian margin, and was connected in the east through a transform to a north (west) dipping subduction zone below the eastern Baleares from which the Kabylides were derived (Figure 2, Scenario 3). In this reconstruction, subduction evolves slowly during the Eocene and has produced a slab length of ~300 km in the Early Oligocene [*Vergés and Fernàndez*, 2012].

4. Four-Dimensional Thermomechanical Modeling of Subduction Evolution

Each of the above reconstruction scenarios are used to define various starting configurations of subduction at ~35 Ma (section 4.3) from which our numerical models of slab evolution will evolve in a dynamic self-consistent way. The experiments aim to test if one, or more, of these starting slab geometries at the inception of rollback would lead to a prediction of the modern mantle structure as imaged by seismic tomography (Figure 3), i.e., after modeling of 35 My of subduction evolution. To this end, we first introduce the 3-D model geometry and the governing transport equations and rheology, after which we explain in more detail our modeling approach of determining the initial condition at ~35 Ma for each reconstruction in terms of temperature field, rheology, and buoyancy.

4.1. Model Geometry and Boundary Conditions

We adopt a regional Cartesian model volume for the western Mediterranean as illustrated in Figure 4. The dimensions of the model box are $1650 \times 1300 \times 1000$ km. The top boundary is free slip and the bottom is no slip. To allow for slab decoupling from the top surface, a weak crustal layer is emplaced on top of the oceanic lithosphere following *Chertova et al*. [2012]. The side boundaries are open for lateral inflow and outflow [*Chertova et al*., 2012], except for the top 150 km of the southern and northern parts of the domain at which kinematic boundary conditions of plate motion will be implemented. Open-side boundaries affect the flow field pattern inside the domain to a much lesser extent than closed, free-slip boundaries [*Chertova et al*., 2012]. This allows to significantly decrease domain dimensions in favor of shorter overall computation time per modeling experiment.

At the top 150 km of the southern and northern sidewalls of the domain, velocity boundary conditions are imposed simulating the relative and absolute plate motions of the African and Iberian (Eurasian) plates. Relative plate motions were taken from the reconstruction of *van Hinsbergen et al*. [2014], which is embedded in the Eurasia-North America-Africa plate circuit of *Torsvik et al*. [2012] and incorporate the recent Iberia-Eurasia reconstruction of *Vissers and Meijer* [2012]. The relative plate motions are placed in the global moving hotspot reference frame of *Doubrovine et al*. [2012] to constrain plate motions relative to the mantle. Considering that the temporal details of this motion are uncertain [*Doubrovine et al*., 2012], we adopt the average plate velocity of the past 35 My as kinematic boundary conditions for our modeling on the southern domain edge in northwest Africa and on the northern edge in northern Iberia. In our models Africa is moving in an almost northern direction (N9°E) with a speed of 8.6 mm/yr, and Iberia is moving in a northeast direction (N58°E) with a speed of 4.6 mm/yr.

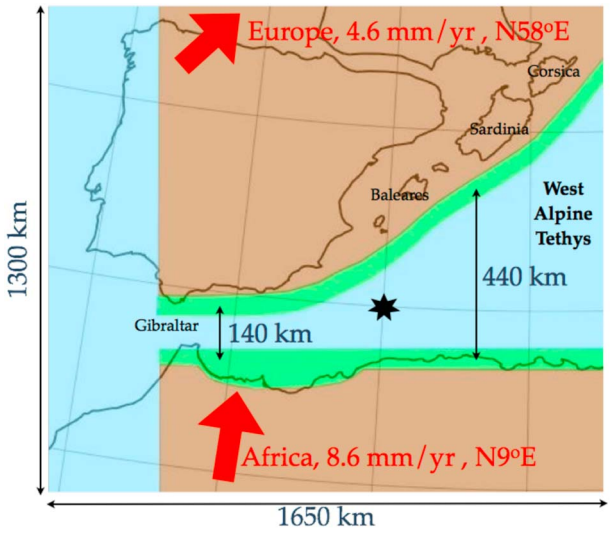

Figure 4. The top view of the modeled region showing the paleogeography at ~35 Ma [after *van Hinsbergen et al*., 2014]. Brown regions are modeled as continental lithosphere, blue regions as oceanic lithosphere, and green regions denote continental margins. Location of active or incipient subduction at ~35 Ma will be indicated in Figure 6. The arrows denote the average absolute plate motion of Iberia and Africa over the past 35 Ma determined from *Doubrovine et al*. [2012]. From the reconstruction of *van Hinsbergen et al*. [2014] we estimate about 140 km of oceanic or transitional lithosphere between Iberia and Africa, and about 440 km between African and the Balearic margin. The average width of continental margins is 70 km. The star shows the position of vertical viscosity profiles in Figure 6.

The paleogeography of the region at ~35 Ma defines the division of the model into continental and oceanic domains and is taken from the tectonic reconstruction of *van Hinsbergen et al*. [2014]. In general, the different reconstruction scenarios agree on the paleogeography (relative distances) at about 35 Ma (Figure 4). As noted above, these scenarios are predominantly different in initial slab geometry and trench location. Figure 4 also shows the subdivision of the lithosphere into oceanic (blue), continental (brown), and continental margin (green) domains. The initial subduction zone geometry for each of the scenarios will be introduced below (Figure 5). In our model the difference between oceanic and continental lithosphere is expressed in the thermal structure and rheology in terms of the strength of the lithosphere. We did not assign a different density to continental lithosphere relative to oceanic lithosphere; hence, there are no lateral buoyancy contrasts, except the contrast corresponding to the initial subducting slab. To the west from Gibraltar, the transition between continental lithosphere of Iberia and Africa, and oceanic lithosphere of the Atlantic Ocean is represented as a NS oriented straight line. This part of the domain was geometrically simplified, as its detailed structure is not of significant influence on the subduction evolution modeled.

The reconstruction of *van Hinsbergen et al*. [2014] determines that ~140 km of oceanic or transitional lithosphere (here modeled as oceanic) separated the paleomargins of Africa and Iberia at the longitude of

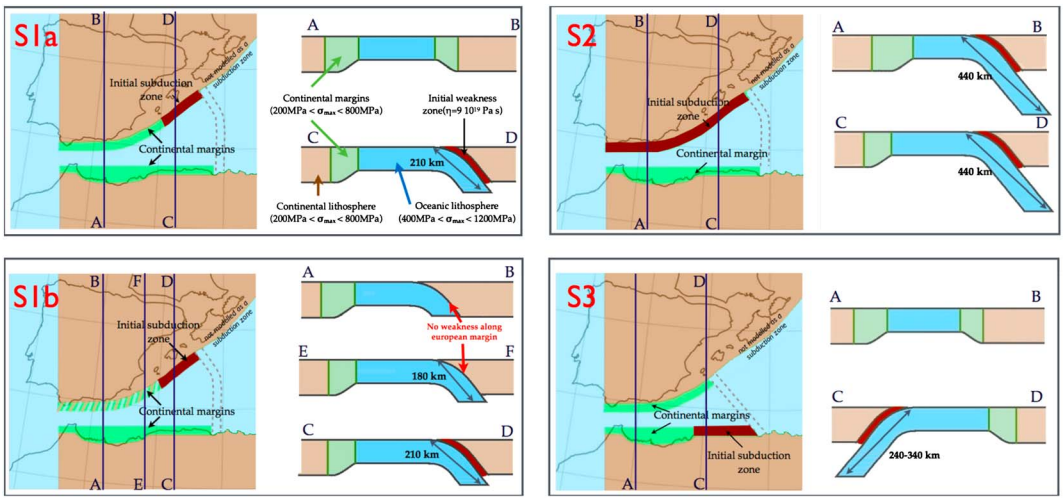

Figure 5. (S1a, S1b) Geometry defining the initial conditions for models with subduction starting under the Balearic margin, under the (S2) whole Iberian-Baleares margin and under the (S3) African margin. The meaning of the colors is as in Figure 4. The fat red lines indicate the initial subduction zone. Vertical cross sections correspond to the NS-lines in the map. The cross sections show the implemented structure of the African and Iberian-Balearic margins for each of the initial models. Dashed lines in the maps depict the transform/decoupling zone represented by weak young lithosphere. For initial configuration, Figure 5 (S1b), the south-Iberian margin is hatched to denote initial thickening.

Table 1. List of Parameters

Symbol	Meaning	Value	Dimension
c_p	Specific heat	1250	$J\,kg^{-1}\,K^{-1}$
k	Thermal conductivity	4.27	$W\,m^{-1}\,K^{-1}$
α	Thermal expansivity	3×10^{-5}	K^{-1}
ρ_0	Reference density	3413	$Kg\,m^{-3}$
Ra	Thermal Rayleigh number, $\rho_0\alpha\Delta T h^3/\eta_0\kappa$	1.7×10^{6}	-
$a\times b\times c$	Dimensions of the model: height, width, length	$1\times1.65\times1.3$	1000 km
η_0	Reference viscosity	10^{21}	Pa s
U_A	African velocity, angle	8, 6; N9°E	$mm\,yr^{-1}$; -
U_E	European velocity, angle	4, 6; N58°E	$mm\,yr^{-1}$; -
γ_1	Clapeyron slope (410 km)	4.1	$MPaK^{-1}$
$\delta\rho_1$	Density contrast (410 km)	273	$Kg\,m^{-3}$
γ_2	Clapeyron slope (660 km)	−1.9	$MPaK^{-1}$
$\delta\rho_2$	Density contrast (660 km)	342	$Kg\,m^{-3}$
η_{LM}	Viscosity of the lower mantle	2×10^{22}	Pa s
A_{diff}	Diffusion prefactor	5.3×10^{15}	s^{-1}
A_{disl}	Dislocation prefactor	2×10^{18}	s^{-1}
V_{diff}	Activation volume for the diffusion creep	4–6	$cm^3\,mol^{-1}$
V_{disl}	Activation volume for the dislocation creep	8–12	$cm^3\,mol^{-1}$
E_{diff}	Activation energy for the diffusion creep	240	$KJ\,mol^{-1}$
E_{disl}	Activation energy for the dislocation creep	423	$KJ\,mol^{-1}$
b	Burgers vector	5×10^{-10}	m
d	Grain size	10^{-6}	m
R	Gas constant	8.314	$J\,mol^{-1}\,K^{-1}$
m	Grain size exponent	2.5	-
n	Stress exponent dislocation creep	3	-
T_0	Normalized surface temperature, $T_{surf}/\Delta T$	0.1605	-
Di	Dissipation number, $\alpha gh/c_p$	0.24	-
Φ	Viscous dissipation	-	$W\,m^{-3}$
γ	Yield stress gradient	0.1–0.6	-
$\dot{\varepsilon}$	Second invariant of the strain rate, $\left(1/2\Sigma_{ij}\dot{\varepsilon}_{ij}{}^2\right)^{1/2}$	-	s^{-1}
v_j	ith component of the velocity	-	-
P	Lithostatic pressure	-	-
$\partial_i\Delta P$	Dynamic pressure gradient, $\partial_i P-\rho_0 g_i$	-	-
τ_{ij}	ijth component of the deviatoric stress tensor, $\eta\dot{\varepsilon}_{ij}$	-	-
T	Temperature	-	-
$\dot{\varepsilon}_{ij}$	Strain rate, $\dot{\varepsilon}_{ij}=\partial_i u_j+\partial_j u_i$	-	-
μ	Shear modulus	80×10^{9}	Pa

Gibraltar at ~35 Ma. To the east, the Alpine-Tethys lithosphere has a north-south extent of up to ~440 km between Baleares and African margin at the longitude of the NBTZ. The width of continental margins is prescribed as 70 km except for the north Moroccan margin, where we allow for wider margin of ~110 km [*van Hinsbergen et al.*, 2014; *Vergés and Fernàndez*, 2012].

4.2. Model Equations

We model the evolution of the western Mediterranean region with the finite element modeling package SEPRAN (http://ta.twi.tudelft.nl/sepran/sepran.html). We solve the following three dimensionless equations (used symbols are given in Table 1) applying the extended Boussinesq approximation for a medium including solid state phase transitions [*Christensen and Yuen*, 1984]:

Mass conservation of an incompressible viscous fluid,

$$\partial_j v_j = 0, \tag{1}$$

the Stokes equation describing force balance,

$$-\partial_i P+\partial_j\tau_{ij}=\left(RaT-\sum\nolimits_k Rb_k\Gamma_k\right)g_i, \tag{2}$$

and the heat conservation equation:

$$\frac{\partial T}{\partial t}+v_j\partial_j T-\partial_j\partial_j T-Di(T+T_0)g_i v_i-\sum\nolimits_k\gamma_k\frac{Rb_k}{Ra}Di(T+T_0)\frac{\mathrm{d}\Gamma_k}{\mathrm{d}t}=\frac{Di}{Ra}\Phi. \tag{3}$$

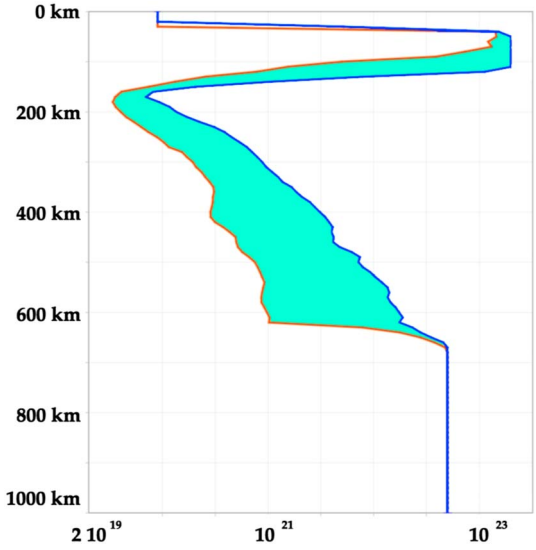

Figure 6. Viscosity profiles in the beginning of the subduction process for models with highest and lowest value for the activation volumes of dislocation and diffusion creep. The depth profiles are taken in the point (marked with a star in Figure 3) with surface coordinates (800 km and 700 km).

The size of the tetrahedral finite elements in our models varies from 7 km at the top to 25 km at the bottom of the model. The number of degrees of freedom for most models is around 3 million. For the modeling of subduction evolution in 3-D, we use parallel computation. The total number of time steps varies between 1500 and 2200. Material properties such as viscosity of the crustal layer and yield strength are defined on particle tracers that are advected with the flow. Tracers were initially randomly distributed inside the modeling domain.

Our models include the two major phase transitions near 410 km and 660 km depth in the unperturbed mantle. The 410 km phase change contributes to the negative buoyancy force and increases slab pull while the phase change at 660 km has a positive buoyancy effect on cold material resisting slab penetration to the deeper mantle [*Christensen and Yuen*, 1984]. Values for the Clapeyron slope and density contrasts are given in Table 1. Phase transitions are parameterized in the model with the phase-transition function:

$$\Gamma_k = \frac{1}{2}\left[1 + \sin\left(\frac{\pi z_{\text{diff}}}{w}\right)\right] \tag{4}$$

where $z_{\text{diff}} = z - ztr - \gamma k \cdot (T - Ttr)$, w is the half-width of k transition zone set to 50 km, ztr and Ttr are the reference depth and temperature of the phase transition, respectively, γk is the Clapeyron slope, and T is temperature [*Čížková et al.*, 2002; *van Hunen*, 2001].

4.3. Rheological Model

A composite viscoplastic rheology is used comprising dislocation and diffusion creep and a simplified plasticity in terms of stress limiting the viscosity (Figure 6)[*Čížková et al.*, 2002; *van Hunen and Allen*, 2011; *Gerya et al.*, 2004; *Schott and Schmeling*, 1998; *Enns et al.*, 2005; *OzBench et al.*, 2008; *Mason et al.*, 2010; *Magni et al.*, 2012]. The effective viscosity η_{eff} is determined as follows:

$$\frac{1}{\eta_{\text{eff}}} = \frac{1}{\eta_{\text{diff}}} + \frac{1}{\eta_{\text{disl}}} + \frac{1}{\eta_y}, \tag{5a}$$

where

$$\eta_{\text{diff}} = \mu\, A_{\text{diff}}^{-1} (b/d)^{-m} \exp[(E_{\text{diff}} + PV_{\text{diff}})/RT], \tag{5b}$$

$$\eta_{\text{disl}} = \mu\ \ A_{\text{disl}}^{-\frac{1}{n}} \dot{\varepsilon}^{\frac{1-n}{n}} \exp[(E_{\text{disl}} + PV_{\text{disl}})/nRT], \tag{5c}$$

and

$$\eta_y = \frac{\tau_y}{2\dot{\varepsilon}} \tag{5d}$$

$$\tau_y = \min(\tau_0 + \gamma P, \tau_{\max}). \tag{5e}$$

In these equations, $\dot{\varepsilon}$ is the second invariant of the strain-rate tensor, $A_{\text{diff, disl}}$ are diffusion and dislocation creep viscosity prefactors, μ is the shear modulus, γ is the yield stress gradient, b is Burgers vector, d is the grain size, m is the grain size exponent, $V_{\text{diff, disl}}$ and $E_{\text{diff, disl}}$ are activation volume and activation energy for diffusion and dislocation creep, respectively, P is the lithostatic pressure, T is temperature, τ_0 is the yield stress value at the top surface, $\tau_{\max}$ is the maximum yield stress value. Parameters for dislocation and diffusion creep are taken for wet olivine (Table 1) [*Karato et al.*, 2001]. The first component of τ_y defines the depth-dependent strength of the material. If the stress exceeds this value the material gradually becomes weaker.

Table 2. List of Models[a]

Model	τ_{max} (MPa) Oc.l.	Cont.l.	Eur.m.	Afr.m.	Subd.z. len. (km)	Kin. Par.	γ	V_{dis}; V_{dif} (cm^3/mol)	Sl.dep. (km)
Scenario 1: Exploring rheology of the mantle and continental margins									
S1.1-1	800	800	800	800	300	D	0.2	8; 5	50
S1.1-2	800	800	100	100	300	D/2	0.1	9; 5	50
S1.1-3	400	800	100	100	300	D/2	0.3	9; 5	50
S1.1-4	1200	800	100	100	300	D/2	0.3	9; 5	50
S1.1-5	400	800	50	50	300	D/2	0.1	8; 4	50
S1.1-6	800	400	100	100	300	D/2	0.1	9; 5	50
S1.1-7	800	200	100	100	300	D/2	0.1	9; 5	50
S1.1-8	800	800	100	100	300	D	0.3	8; 4	50
Scenario 1: Exploring the strength of the Iberian margin									
S1.2-1	800	800	800	100	250	D	0.2	8; 4	50
S1.2-2	800	800	800	200	250	D	0.3	8; 4	50
S1.2-3	1000	1000	1000	200	250	D	0.5	8; 4	50
S1.2-4	1000	1000	1000	50	250	D	0.6	8; 5	50
Scenario 1: Increasing Iberian margin thickness									
S1.3-1	800	800	200	100	800	D	0.3	8; 4	50
S1.3-2	800	800	800	100	250	D	0.3	8; 4	50
Scenario 2: Initial N-NW directed subduction from Gibraltar to the Baleares									
S2.1-1*	800	800	50	50	800	D/2	0.1	8; 4	200
S2.1-2	800	800	50	50	800	D/2	0.1	8; 4	200
S2.1-3	800	800	200	200	800	D	0.3	9; 5	200
S2.1-4	800	800	200	800	800	D	0.3	11; 6	200
Scenario 3: Initial S-SE dipping subduction under the African margin									
S3.1-1	800	800	200	200	400(AM)	D	0.3	8; 4	150
S3.1-2	800	800	800	200	400(AM)	D	0.3	9; 4	150
S3.1-3	800	800	800	200	400(AM)	D	0.5	10; 5	150
S3.1-4	800	800	800	800	400(AM)	D	0.5	12; 6	150
S3.1-5	800	800	800	800	400(AM)	D	0.3	10; 5	60
Scenario 1: Sensitivity of subduction models to variations in initial conditions									
S1.4-1	800	800	800	100	250	D	0.3	8; 4	90
S1.4-2	800	800	800	100	250	D	0.3	8; 4	50
S1.4-3*	800	800	800	100	250	D	0.3	8; 4	60
S1.4-4*	800	800	800	100	250	D	0.3	8; 4	50
S1.4-5*	800	800	800	100	250	D	0.3	8; 4	50
S1.4-6	800	800	300	100	250	D	0.3	8; 4	50
S1.4-7*	800	800	800	100	250	D	0.3	8; 4	50

[a]Models marked S1.*, S2.*, or S3.* are computed for tectonic scenarios S1, S2, or S3, respectively. Oc.l. and Cont.l. means oceanic and continental lithosphere, respectively, Eur.m. and Afr.m—European and African margin, Vdis and Vdif activation volumes for the dislocation and diffusion creep and Kin. Par.—kinematic parameters implemented to the African and European plates. Models marked with asterisk depend on additional parameters which are not included in this table. For the description of these models, see text.

The strength of the material increases with depth until it reaches τ_{max}. Within the slab this strength limitation results in weakening of the slab in the bending zone accommodating subduction and rollback.

In our modeling we experimented with different rheological parameters. The rheology was defined in each experiment by setting values for the activation volume for dislocation and diffusion creep as well as for τ_{max} and μ to define the stress limiting of viscosity. The activation volume was varied between 4 and 6 $cm^3\,mol^{-1}$ for diffusion creep and 8–12 $cm^3\,mol^{-1}$ for the dislocation creep, respectively, and the strength of the material defined in terms of τ_{max} was varied in the range of 50–1200 MPa for different parts of the model and in different experiments as was also done by others [*Alisic et al*., 2012; *van Hunen and Allen*, 2011]. This allowed us to experiment with weak and strong continental margins in combination with weak or strong slabs evolving through a weak or strong ambient mantle. The strength of the continental lithosphere was also defined by a maximum yield stress value and was varied between 200 and 800 MPa. The rheological strength of the continental margins is essentially unknown. Margin strength was varied between experiments and preset in each experiment with the value of τ_{max} ranging between 50 and 800 Mpa (Table 2).

To illustrate the typical range in upper mantle viscosities resulting from these parameter variations, we show in Figure 6 the average difference between viscosity profiles for the models with strong and weak ambient mantle rheology at the beginning of the subduction process just before the development of fast rollback. These profiles are taken in the "undisturbed" part of the domain, i.e., far from the subduction zone (marked with a star in Figure 4) where strong strain rate variations may determine rheology. The blue line shows the viscosity profile for a model with strong rheology using $V_{diff} = 6\,cm^3\,mol^{-1}$ and $V_{disl} = 11\,cm^3\,mol^{-1}$. The orange line corresponds to the viscosity profile for a similar model experiment but with a weak rheology using $V_{diff} = 4\,cm^3 mol^{-1}$ and $V_{disl} = 8\,cm^3 mol^{-1}$. The lower mantle viscosity for these two models was set to 5×10^{22} Pa s following *Čížková et al.* [2012]. The minimum viscosity allowed is set to 1×10^{19} Pa s and maximum viscosity is set to 10^{24} Pa s [*Magni et al.*, 2012; *Garel et al.*, 2014]. We refer to *Chertova et al.* [2012] for illustrations of viscosity field evolution typical for subduction evolution as is modeled here.

The viscosity of the weak crustal layer that allows slab decoupling from the top free-slip surface was taken as 9×10^{19} Pa s and its thickness is 30 km. Here we follow the approach of *Čížková et al.* [2007], *OzBench et al.* [2008], *Stegman et al.* [2010], *Chertova et al.* [2012], and *Capitanio and Replumaz* [2013].

4.4. Initial Conditions

The three tectonic reconstruction scenarios essentially start from different initial subduction zone configurations at ~35 Ma. These were translated here into initial temperature conditions for 3-D modeling. In Figure 5 we display four setups of initial configurations for scenarios S1, S2, and S3, where S1a and S1b are alternative starting configurations for S1, which will be discussed below (section 5.1.3). In addition to the map view display of Figure 4, thick dark red zones indicate the location of the subduction zone at ~35 Ma. Vertical cross sections depict the character of the margins, passive or subduction, and amount of initial subduction.

We assumed an initial subduction "channel" of 40 km filled with a weak material with a viscosity of 9×10^{19} Pa s [*van Hunen and Allen*, 2011; *Chertova et al.*, 2012]. The relatively large width of the subduction channel is not critical [*Chertova et al.*, 2012] and only facilitates decoupling of the slab and overriding plate in the initial few million years of subduction in the presence of advancing African motion before active subduction turns into a regime of predominant slab rollback.

The dashed lines in Figure 5 between the Baleares and African margins represent a weakness zone which separates the oceanic lithosphere of the RGB slab in the west from the lithosphere that will rollback to the southeast and east [*Spakman and Wortel*, 2004]. The subduction that occurred to the east of the decoupling zone is not incorporated in the main modeling effort here, although we will show one model in which we took the Kabylides segment into account. For all scenarios, the decoupling zone is implemented as a narrow (70 km) region filled with thin young oceanic lithosphere (5–50 My), although in reality it may have been an inherited transform fault that formed during the Jurassic opening of the Alpine Tethys. This lithosphere acts as a weakness zone due to its temperature-determined rheology at shallow depths. To the east of this decoupling zone we have implemented a 100 My old oceanic plate.

Although we model the Alpine-Tethys lithosphere as being of oceanic origin, its precise character is unknown. It is Jurassic to earliest Cretaceous in age [*Vissers et al.*, 2013], but it cannot be excluded that the now subducted domain was (partly) of transitional nature resulting from thinning of continental lithosphere, which subsequently cooled and thickened similar to oceanic lithosphere in terms of thickness and temperature structure. The initial temperature profile of the oceanic/transitional lithosphere is determined from the equation of cooling of a semiinfinite half space for a lithosphere age of 100 My, equivalent to an earliest Cretaceous lithosphere age consistent with the age of the end of spreading of the Alpine Tethys Ocean [*Vissers et al.*, 2013]. A constant temperature gradient of 10 K/km is prescribed for the continental lithosphere across its thickness of 150 km.

4.4.1. Scenario 1: Initial Subduction Confined to the Balearic Margin (Models: S1.*)

The initial geometry for S1 is quantified from the recent reconstruction of *van Hinsbergen et al.* [2014] and presented in Figure 5 (S1a). At ~35 Ma, the initial trench is 300 km long and located south of the Balearic Islands. In the east, the initial slab length is ~200 km from the surface. This decreases to 0 km below the base of the lithosphere close to the Iberian margin just west of cross section CD in Figure 5 (S1a). The initial subduction direction is NW with an assumed dip angle of 40°.

The thickness of both European and African continental margins is gradually increasing toward the interior of the continents. We experimented with different initial settings of maximum yield stress (equation (5e)). Weak margins were defined by $\tau_{max} = 50 - 200$ MPa and strong margins by $\tau_{max} = 400 - 800$ Mpa.

For the continental margin of south Iberia we also experimented with different initial margin geometries (Figure 5). Between 80 Ma and 35 Ma, convergence between Africa and south Iberia was not more than a few tens of kilometers [*van Hinsbergen et al*., 2014] and may have led to thickening of the south Iberian margin. We mimicked the margin thickening by a gradual increase in margin thickness from 0 km at Gibraltar to ~30 km at the transition to the Baleares margin as depicted in Figure 5 (S1b). This led to a mechanically stronger margin for which we could still vary the maximum yield stress τ_{max}.

4.4.2. Scenario 2: Initial Subduction Along the Entire Iberian-Balearic Margin (Models S2.*)

Scenario S2 assumes an initial subduction zone of 900 km along the entire Iberian margin from the Gibraltar to the Baleares (Figure 5 (S2)). We experimented with models starting from an initial length of the slab of ~400 km all along the Iberian-Baleares margin and with models in which the depth of the slab below the base of the lithosphere increases linearly from 0 at Gibraltar to ~300 km at the eastern Baleares as end-member models for scenario S2. The initial subduction direction was north at Gibraltar, gradually changing to northwest under the Balearic margin with a subduction angle of ~40°.

4.4.3. Scenario 3: Initial SE Dipping Subduction Under the North African Margin (Models S3.*)

Initial conditions of a S dipping subduction zone under the African margin are shown in Figure 5 (S3). At ~35 Ma, the length of initial slab was ~300 km with an initial subduction angle of ~45°. The trench started at the north African margin ~300 km to the east from the (future) Moroccan Rif. Between the Rif and the trench a wide continental margin (110 km) was prescribed [*Vergés and Fernàndez*, 2012; *van Hinsbergen et al*., 2014]. Along southern Iberia we prescribed a continental margin of which the strength is controlled by τ_{max}.. The geometry of the weak decoupling oceanic transform zone (dashed in Figure 5 (S3)) is taken from *Vergés and Fernàndez* [2012] and was located more to the west than in S1 and S2, excluding most of the Balearic margin.

4.5. Criteria for Model Evaluation, Modeling Targets, and Optimization Strategy

Our primary target for model evaluation is prediction of the observed present-day mantle structure. However, current tomography models are not perfectly resolved [*Spakman and Wortel*, 2004; *Bezada et al*., 2013] and lead to a blurred view on mantle structure. Therefore, we compare predictions of slab morphology to the robust features of the imaged slab anomaly, which we identified as the curvature and position of the slab (section 2 and Figure 3). These targets should be reached after 35 My of subduction evolution starting from the initial conditions defined above. We note that observations and interpretations of present-day mantle anisotropy [e.g., *Diaz et al*., 2010; *Alpert et al*., 2013; *Díaz and Gallart*, 2014] and of crustal motions [e.g., *Vernant et al*., 2010; *Koulali et al*., 2011] are not taken here as particular modeling targets because the sensitivity of these observations for the past 35 My of subduction evolution is unknown.

The temporal evolution of subduction is another important constraint. An intermediate milestone for all numerical models is that slab rollback largely stalls at ~8 Ma as suggested by earlier mentioned geological constraints. For S1 and S2 an intermediate target is the collision of the Kabylides with Africa (~15–17 Ma), which corresponds to rollback of the easternmost part of our modeled slab having reached the African margin.

Our models started with the initial buoyancy field as described in the previous sections. Slab buoyancy and the prescribed plate motions at the south edge and north edge of the model domain drive the subsequent subduction evolution. As the rheology of the mantle, slab, and margins is poorly known we tuned these for different model regions (by varying parameters in equation (5)) to optimize for each reconstruction scenario the possibility for the end stage of slab evolution to approximate the real-Earth targets.

5. Experiments

A summary of important models is given in Table 2. The models are divided into six groups, each serving a particular modeling objective. Model names start with the scenario identifier S1, S2, or S3.

5.1. Scenario 1: Initial Subduction Confined to the Baleares Margin

We started our experiments with modeling the subduction evolution based on S1. This is the most complex evolution scenario and involved a large number of experiments to explore the plausible range of parameters

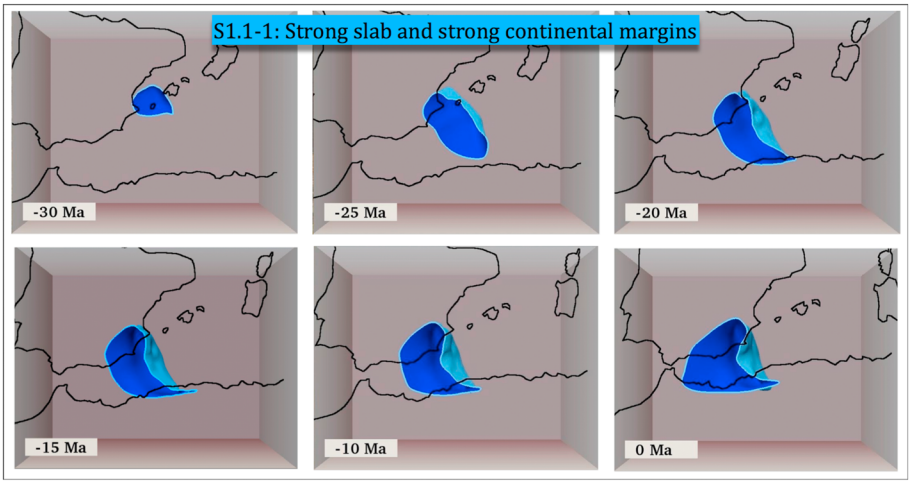

Figure 7. Evolution of the model S1.1-1. The 1400°-isotherm of the slab is shown in light blue below 150 km. Dark blue shows the interior of the slab. Black contours indicate the paleo-coastlines of North Africa, Iberia, the Balearic Islands, and of Corsica and Sardinia. These were linearly interpolated between their position at 35 Ma and the present. These coastlines only serve to illustrate the approximate plate position of the African and Iberian continents with respect to the slab.

for mantle viscosity and strength of the continental margins. From this experience we benefited in modeling the subduction evolution for tectonic scenarios S2 and S3.

5.1.1. Exploring Rheology of the Mantle and Continental Margins

From an initial condition of a short slab, extending ~50 km under the Balearic lithosphere (Figure 5 (S1a)), all models (Table 2) start to roll back, initially to the south and subsequently quite rapidly rotating to the west. The transition between the Iberian margin and Balearic subduction zone initially acts as a pivot point about which rollback rotates to the west. For a strong slab, the strength of the margin at this point determines whether the margin starts to fail (weak margin) or whether it will act against further rollback (strong margin). These observations are also valid for tearing of the north African margin accommodating westward rollback.

Model S1.1-1 (Figure 7) is an example of a model with a strong Iberian and African margin (τ_{max} = 800 MPa) and a strong slab (τ_{max} = 800 MPa). During the first 5 My, the slab under the Baleares margin subducts another ~50 km in northwest direction (Figure 7, 30 Ma) with relative convergence speed of 6 mm/yr, followed by increasing rollback to the southwest. Such a rapid transition is also observed in other numerical and laboratory experiments [*Becker et al.*, 1999; *Faccenna et al.*, 2001b; *Schellart and Moresi*, 2013]. When the trench reaches the African margin at ~25–20 Ma, rollback only occurs westward. No appreciable tearing occurs in the slab or along the margins during the last 20 Ma of evolution. Slab rollback gradually stagnates while the slab thickens due to ongoing Africa-Iberia convergence. At 0 Ma, a wide, shallow anomaly is observed far from the present-day slab position under the Gibraltar and this model does not reach the modeling target.

To allow the slab to progress farther to the west, we first tried models (not in Table 2) with weaker slabs and weaker margins with $\tau_{max\_slab} = \tau_{max\_margin}$ on the order of 200–300 MPa (equation (5e)). In these models, margins start to drip from the strong (800 MPa) continents, large holes form in the slab and it experiences major down-dip stretching during the entire evolution, particularly when its base reaches into the more viscous transition zone (410–660 km) while the upper part continues to retreat to the west (Figure S1 in the supporting information). Remnants of slab in this model are found under the entire Alboran-Algerian basin, inconsistent with tomography observations. From these experiments we concluded that we should proceed with the combination of a relatively strong slab to suppress slab stretching and a weaker continental margin to facilitate tearing.

With the next generation of models (S1.1-2, S1.1-3, S1.1-4, and S1.1-8) we tested different strengths of the oceanic lithosphere and upper mantle in combination with weak continental margins (τ_{max} = 50 or 100 MPa) (Table 2). In most models we used reduced plate velocities due to initial underestimation of the plate velocities. The best performing of these models is model S1.1-8 for which we used a strong (800 MPa) slab and a weak

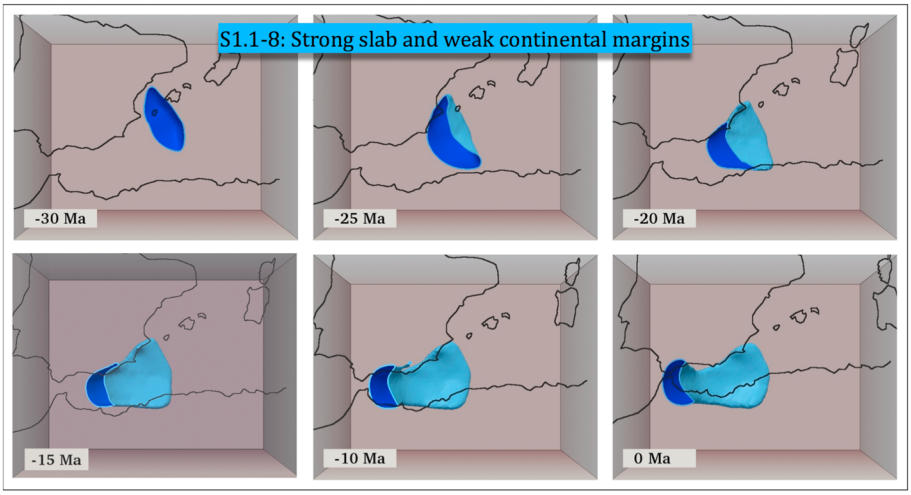

Figure 8. The evolution of the model S1.1-8 shown from a depth of 200 km. See caption of Figure 7 for other descriptions.

mantle ($V_{diff} = 4\ cm^3\ mol^{-1}$, $V_{disl} = 8\ cm^3\ mol^{-1}$). Its subduction evolution (Figure 8) shows a slab arriving in the present-day target region of Gibraltar. After an initial stage (35–30 Ma) of nearly stationary subduction, fast rollback develops to the SW and later to the west. When the trench reaches the African margin, lithosphere tearing starts to propagate to the west along the African and Iberian margins, creating slab edges and associated STEP faults [*Govers and Wortel*, 2005], accommodating subsequent westward rollback. Slab tearing occurs as a viscous necking process of the weak continental margin [*Andrews and Billen*, 2009; *Mason et al.*, 2010; *Duretz et al.*, 2011; *Duretz and Gerya*, 2013; *van Hunen and Allen*, 2011]. The final trench position in model S1.1-8 is slightly to the west and south of the modeling target, and we do not observe the curved morphology of the slab under the Betic region (Figure 3). Instead, the slab lies under the Alboran and Algerian basins, inconsistent with tomographic models.

To illustrate the influence of mantle and slab strength on the subduction evolution, a west-east cross section of model S1.1-8 is shown across the Gibraltar Strait in the end stage (0 Ma) in Figure 9 together with the final slab geometry attained in models S1.1-2 and S1.1-4. Compared to model S1.1-8, model S1.1-2 has a weaker slab (defined in terms of a relatively low $\gamma = 0.1$) and a stronger mantle ($V_{diff} = 5\ cm^3\ mol^{-1}$, $V_{disl} = 9\ cm^3\ mol^{-1}$). As a result the weak slab did not reach the present-day position after 35 My of subduction. In model S1.1-4 we used a stronger slab (1200 MPa) than in model S1.1-8 and a stronger mantle restricting slab rollback to a position ~200 km east of Gibraltar. An experiment with a strong slab in a weak mantle led to complete detachment of the slab at ~15 Ma far east of Gibraltar as the weak margins and mantle could not sufficiently support the weight of the slab (Figure S2 in the supporting information).

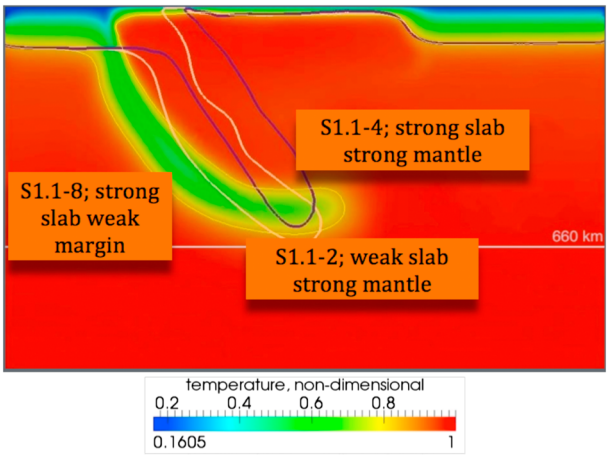

Figure 9. W-E cross section of the temperature field of the model S1.1-8 after 30 Ma from the beginning of the subduction. The 1400°-isotherm for three models is shown. Colors denote the temperature field of model S1.1-8.

Two experiments, S1.1-6 and S1.1-7, were performed to investigate the influence of the continental strength on subduction evolution. In these experiments, τ_{max} was reduced by factors 2 and 4, respectively, from the reference value of $\tau_{max} = 800$ MPa. The mantle in these experiments was strong (activation volumes are 5 and $9\ cm^3\ mol^{-1}$), the slab was weak ($\gamma = 0.1$). Reduction by a factor of 2 did not influence

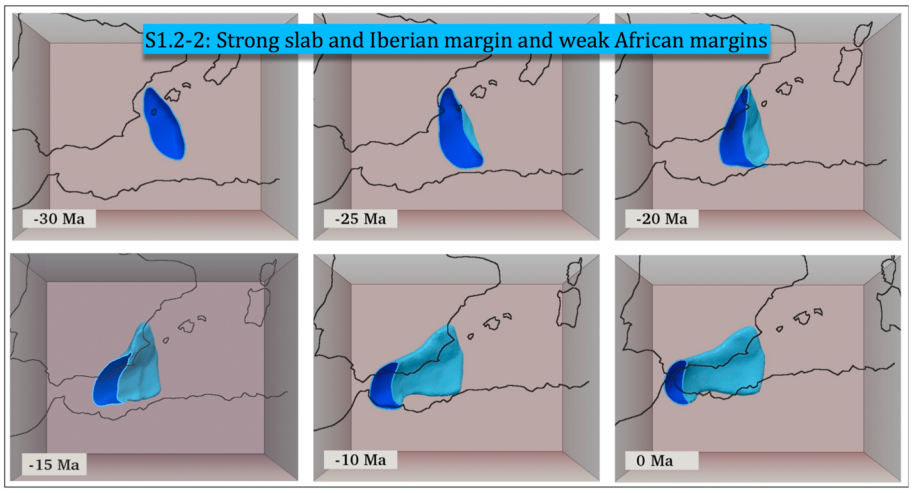

Figure 10. The evolution of the model S1.2-2 is shown below 200 km. See the caption of Figure 7 for other descriptions.

the overall character of the rollback process but with a reduction by a factor 4, the continental lithosphere of Africa became involved in the subduction process, which is not observed in margin geometry or in mantle structure inferred by tomography (Figure S3 in the supporting information).

Based on this group of experiments we continued our experiments with slab strength of 800 MPa and a weak African margin (~50–200 MPa).

5.1.2. Exploring the Strength of the Iberian Margin

As a result of tearing of the Iberian margin and westward rollback, none of the previous models yielded a slab evolution that incorporated ongoing clockwise rotation of the northern sector leading to the E-W trending slab underneath the eastern Betic region (Figure 3). With the second group of S1.* models in Table 2 we investigated the potential role of the south-Iberian margin west of the Baleares in causing slab rotation. We tested different values of τ_{max} for the Iberian margin and for oceanic lithosphere, as well as different values for γ, which influences the depth-dependence of τ_y (equation (5e)).

The first two models, S1.2-1 and S1.2-2 (Figure 10), using the strength of 800 MPa for the Iberian margin, showed a similar subduction evolution as model S1.1-8 (Figure 8) while the last two models, S1.2-3 and S1.2-4, show less trench retreat. The initial evolution was similar to S1.1-8 until the strong Iberian margin locally restricted rollback leading to a clockwise rotation of the slab (25–15 Ma). However, eventually the Iberian margin started to tear, which restored the N-S strike of the trench, leading to an end stage of rollback similar as for S1.1-8.

We conclude that rheological strengthening of the continental margin along Iberia alone does not lead to the observed curvature and location of the slab as portrayed in tomography.

5.1.3. Increasing Iberian Margin Thickness

We subsequently tested the effect of a thickened Iberian margin (Figure 5 (S1b), section 4.4.1), which provides additional strength to the margin independent of its rheological/material strength. Variation of rheological parameters started from those used for model S1.1-8 (Figure 8). In model S1.3-1 the strength of the thickened European margin was 200 MPa. The model developed similar to S1.2-group of models and was not successful in preventing early lithosphere tearing under Iberia.

Next, a strong 800 MPa and thickened European margin (Figure 5 (S1b)) was used leading to model S1.3-2 (Figure 11). Until 25–20 Ma this model is similar to S1.2-2 (Figure 10), after which the slab stayed connected to the Iberian margin and consequently rotated clockwise into the curved geometry as observed in the mantle today. At ~10 Ma the slab reached its present-day position with little change in slab morphology until 0 Ma. Viscous necking of the subducted Iberian margin lithosphere was incipient during the last 10 My, but did not evolve into a detachment under the eastern Betic region as is observed in tomography. Apart from that, the present-day trench position and continuous Gibraltar slab, the slab edge under the Moroccan Rif, the curved slab structure under the Betics, as well as the deeper slab structure successfully reproduced the

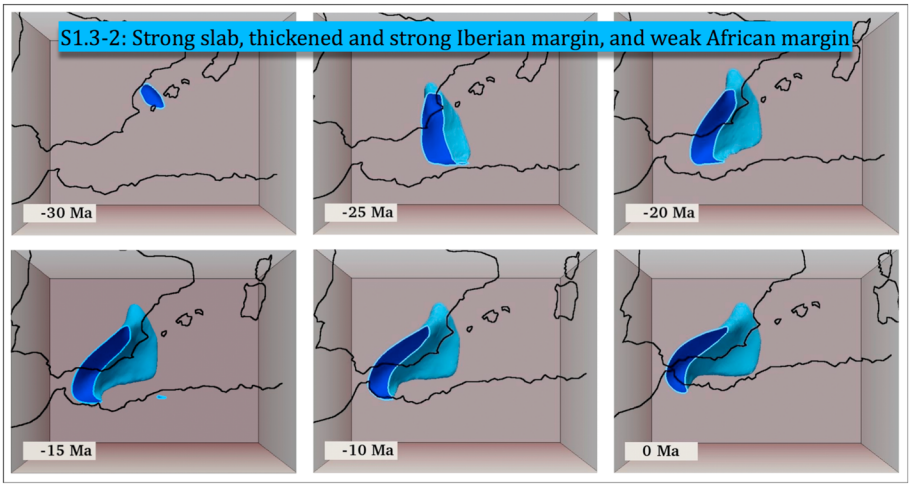

Figure 11. The evolution of the model S1.3-2 is shown below 200 km. See the caption of Figure 7 for other descriptions.

tomographically imaged structure of the RGB slab (Figure 3) [*Spakman and Wortel*, 2004; *Bezada et al*., 2013; *Palomeras et al*., 2014].

5.2. Scenario 2: Initial N-NW Directed Subduction From Gibraltar to the Baleares

Within the parameter space as determined in the previous sections, we now test whether the initial conditions of Scenario 2 (Figure 5 (S2), section 4.4.2) could also evolve into the present-day slab geometry inferred by tomography.

In a first configuration, a slab was implemented with an along-strike varying initial depth from 0 km below base of the lithosphere at Gibraltar to ~300 km below the Baleares. This initial setting led to subduction evolution model S2.1-1 (Figure 12; Table 2) with a rollback evolution similar to models like S1.2-2 (Figure 10) although tearing now only occurred along the African margin. After a short phase (4–5 My) of stationary subduction, fast rollback developed in a southwest direction and evolved quicker than previous models because of the longer initial slab length toward the NE (Baleares). From ~30 Ma to ~15 Ma, the trench retreated in a SW direction until it reached the Gibraltar region. The resulting shape of the trench is comparable to models S1.1*–S1.2*, but is rotated more in anticlockwise direction and located more to the south relative to these models. This resulted from a higher degree of southward rollback with subduction of African continental subduction during the last few million years. The final slab morphology predicts the first

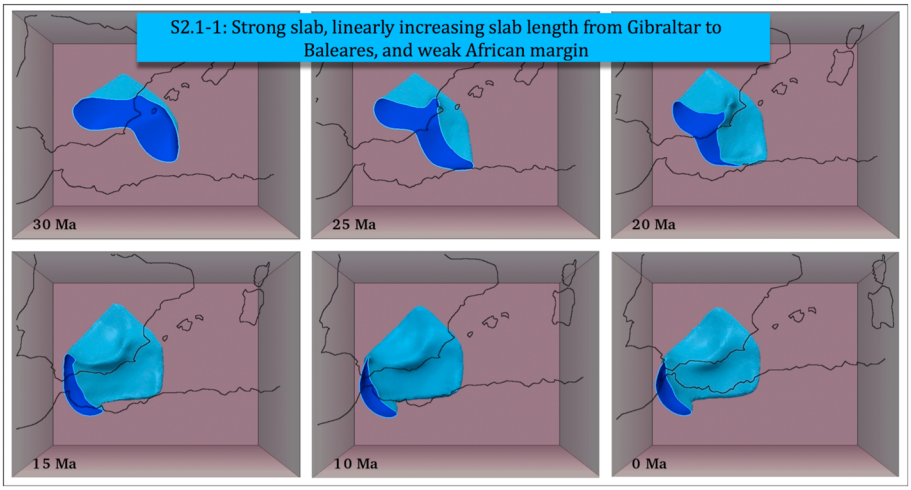

Figure 12. Evolution of the model S2.1-1 is shown below 200 km. See the caption of Figure 7 for other descriptions.

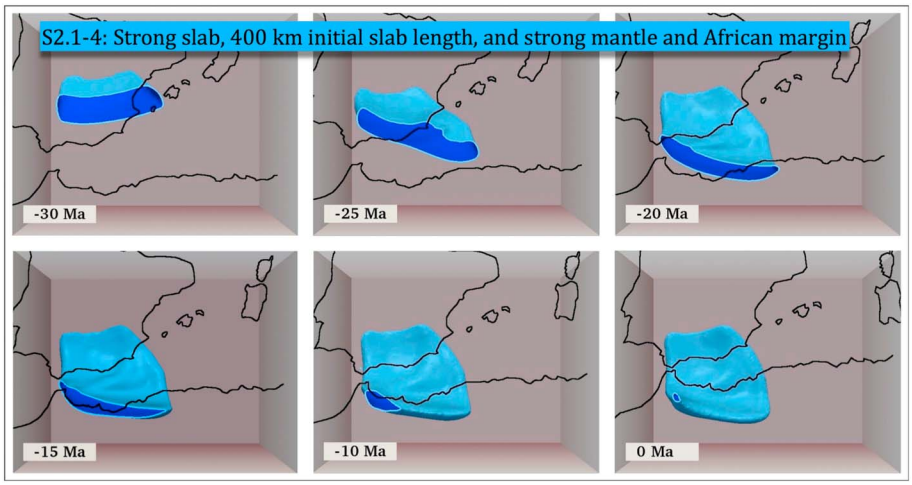

Figure 13. Evolution of the model S2.1-4 below 200 km. See the caption of Figure 7 for other descriptions.

300–400 km of slab to be positioned largely under northern Africa. In addition, slab in the upper mantle transition zone is predicted under the Alboran and west Algerian basins as well as under southern Iberia. This slab morphology is not observed in tomographic models (section 2).

The second slab configuration we tested consisted of a uniform initial slab length of ~400 km along the entire Iberian-Baleares margin (Figure 5 (S2)). This initial configuration was tested in models S2.1-2, S2.1-3, and S2.1-4, which differed in African margin strength and in increasingly stronger mantle rheology, respectively (Table 2). Model S2.1-2, with a weak African margin, exhibited fast rollback to the south and the slab completely detached from the surface after 15 My of the evolution. After 30 My, the detached slab was lying entirely on the 660 km boundary. For the part of the slab at the transition to Atlantic lithosphere in the Gibraltar region we observe fast lithosphere tearing in a southward direction, despite the 800 MPa strong Atlantic lithosphere of this region. The resulting slab geometry is not observed in the present-day mantle.

With the next two models, S2.1-3, and S2.1-4 (Figure 13), we attempted to suppress early lithosphere tearing by tuning the strength of the mantle and African margin targeted at optimizing the correlation between predicted and observed slab structure. These attempts were not successful. The large initial buoyancy force of the 400 km long slab produced fast mantle flow and high strain rates locally reducing the viscosity in the asthenosphere as a result of strong nonlinear dislocation creep (equation (5c)). Counteracting this behavior was possible through strengthening the mantle rheology by using higher activation volume values for diffusion and dislocation creep than those used for models of the S1-group, e.g., S1.3-2 (Figure 11). Slab evolution is illustrated through the last model S2.1-4 (Figure 13) in which the African continental margin and the oceanic plate have the same strength and the mantle is strongest. This model yielded slower rollback than in model S2.1-2, but nevertheless, after 35 My of subduction evolution the slab is almost detached. Due to a stronger continental margin than that in S2.1-2, the tearing zone for this model is now localized within the subducted slab instead of the continental margin. For scenario S2 we found no combination of initial slab geometry and margin/slab/mantle rheology that would lead to an end stage comparable to the present-day slab geometry (Figure 3). In particular, none of the models show a tendency to create a slab curvature from N-S at Gibraltar to E-W below southern Iberia between depths of 0 and 400 km.

5.3. Scenario 3: Initial S-SE Dipping Subduction Under the African Margin

Lastly, we tested whether modern mantle structure can be obtained by starting from the initial conditions of Scenario 3 (Figure 5 (S3), section 4.4.3). Initial slab length is ~300 km. The first model S3.1-1 (Figure 14) implemented strength of 200 MPa for continental margins and 800 MPa for lithosphere (Table 2). In the first 4–5 My, stationary subduction gradually turned into a northward rollback regime followed by rapid rollback in the following ~5 My in predominantly northern direction. Next, lithosphere tearing developed along the weak Iberian margin and the direction of the rollback rapidly changed to westward. After 18–20 My the trench reached Gibraltar with a N-S strike of the trench. The rollback process slowed down and stopped after

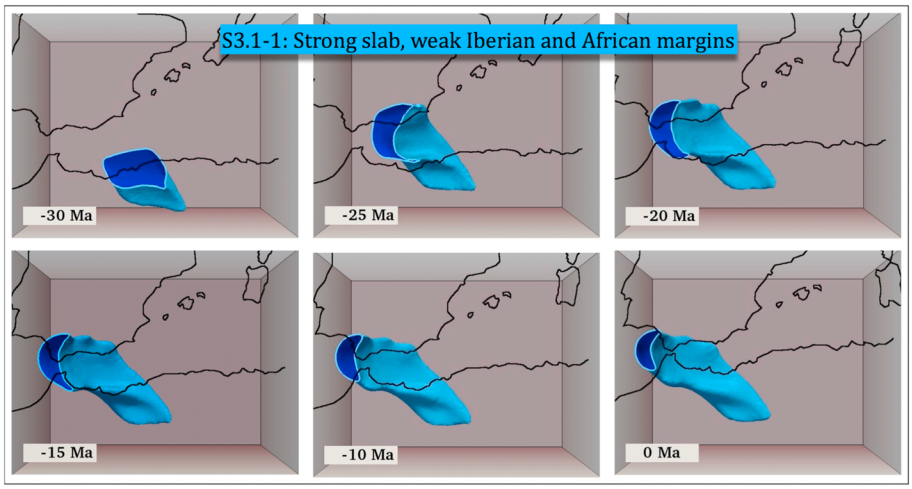

Figure 14. Evolution of the model S3.1-1 below 200 km. See the caption of Figure 7 for other descriptions.

30 My of subduction evolution with a trench located west of Gibraltar. No slab curving under southern Iberia is predicted in this model.

For the next experiments we increased the strength of the European margin to prevent lithosphere tearing and generate bending. The values for the activation parameters as well as γ for τ_y were also increased to provide more mantle support for the slab and suppress fast lithosphere tearing along the Iberian margin. The best performing model (S3.1-4) is shown in Figure 15a. Subduction evolution up to 20 Ma is similar to S3.1-1 with initial slow subduction followed by a rollback in the northerly direction. After reaching the Iberian margin, no lithosphere tearing occurred. Although in the uppermost mantle the trench and the slab have a curvature consistent with tomographic constraints, the deep part of the slab reaches far below the African plate, which is inconsistent with tomographic constraints (Figure 3).

As an attempt to improve the correlation between the modeled and observed slab at depths $>$200 km, we decreased the initial length of the slab at 35 Ma by ~100 km so as to suppress deep mantle resistance to the slab rollback and allow farther slab propagation to the north. In the end stage of this model, the slab is still located under northern Africa partly because of the northward motion of the Africa plate overriding the deep slab since the start of rollback (Figure 15b). Although tectonic evolution scenario S3 comes closer to predicting the observed shallow mantle structure, a good fit between the overall predicted and observed slab morphology could not be achieved by varying the rheology, margin attributes, or initial slab geometry.

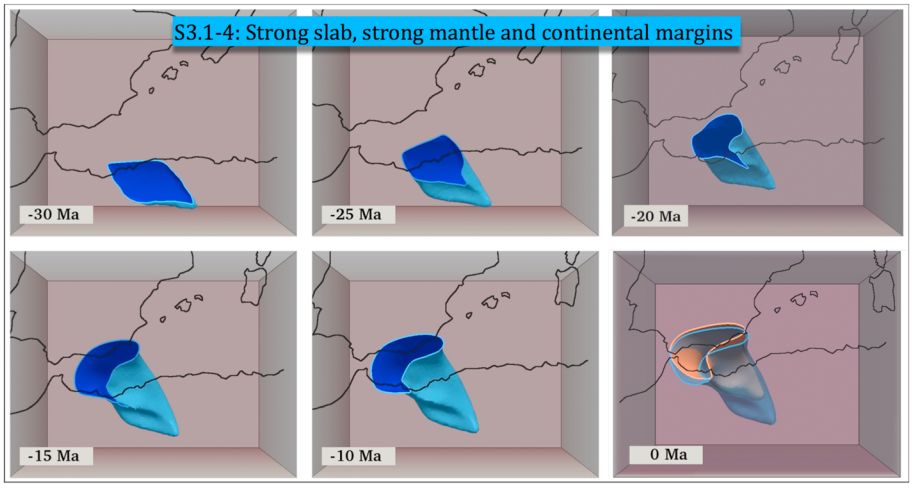

Figure 15. Evolution of the model S3.1-4 (blue) below 200 km. In the last snapshot (0 Ma) two models S3.1-4 and S3.1-5 are shown. The last model, S3.1-5 is shown in orange color. See the caption of Figure 7 for other descriptions.

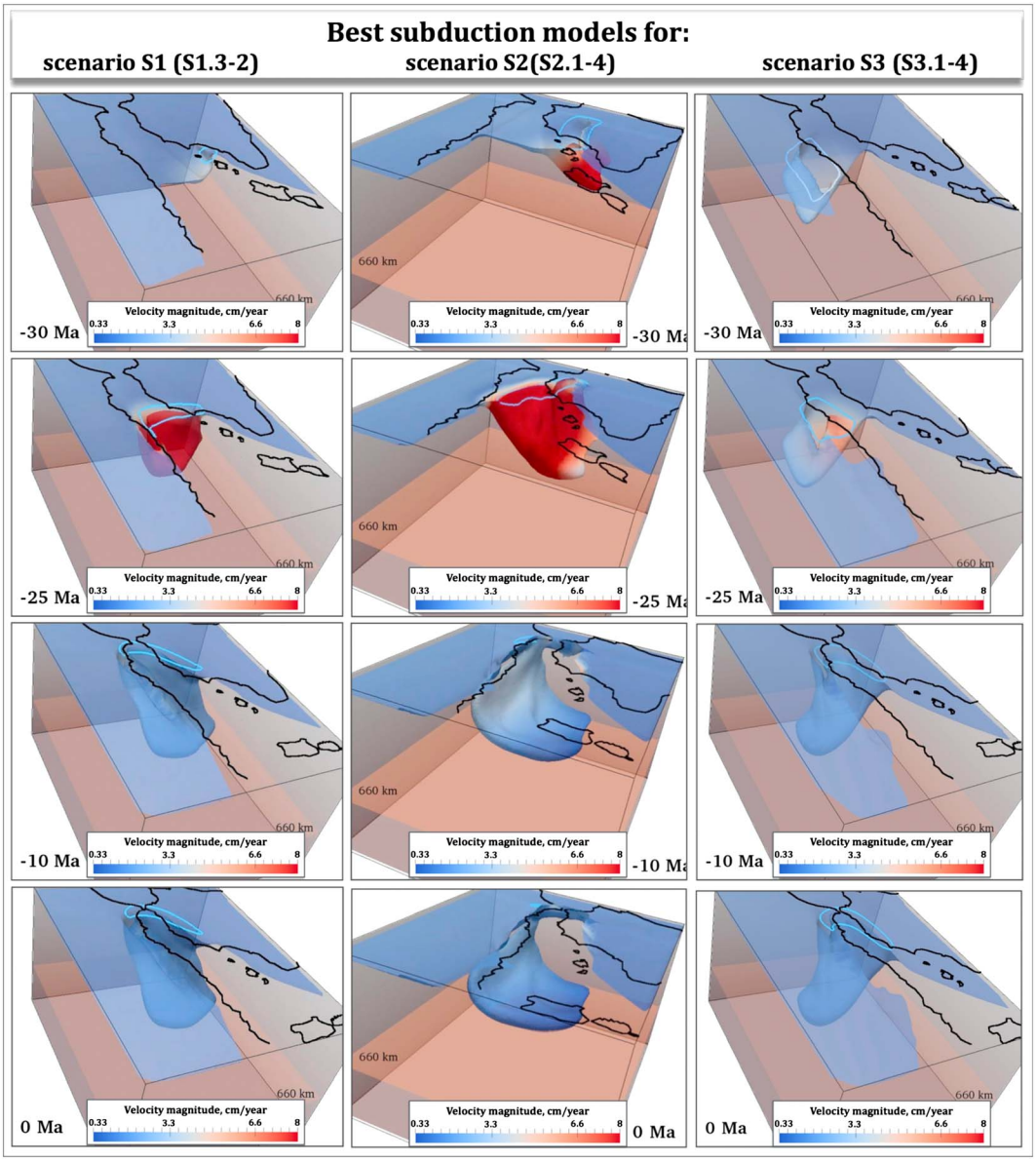

Figure 16. Three-dimensional view on the evolution of the best model obtained for each reconstruction scenario. (left) Scenario S1, model S1.3-2, starting from a short trench at the Baleares margin. (middle) Scenario S2, model S2.1-4, starting from a long initial subduction zone and long slab. (right) Scenario S3, model S3.1-4, starting from a trench at the African margin. For S1.3-2 and S3.1-4 the view is from the southeast, and for model S2.1-4 the view is from the northeast. Blue contours at the surface show the shape of the cold anomaly at depth of 200 km.

6. Discussion and Additional Experiments

6.1. Comparison of the Best Fitting Subduction Models of Each Tectonic Scenario

Our experiments demonstrate that the initial subduction configurations of the three different tectonic evolution scenarios lead to distinctly different subduction evolution of which the end stage of slab morphology can be compared to the present-day mantle structure. Figure 16 shows from each tectonic scenario the subduction model that best fitted present-day mantle structure, i.e., S1.3-2 (Figure 11), S2.1-4 (Figure 13), and S3.1-4 (Figure 15). In all models we observe an initial phase of fast rollback which reduces in speed once the slab entrains the deeper and viscous mantle and even more when the slab comes into contact with the viscosity increase across the 660 km discontinuity, similar to those observed in laboratory experiments [*Faccenna et al.*, 2001b]. The subduction process developed initially much faster for

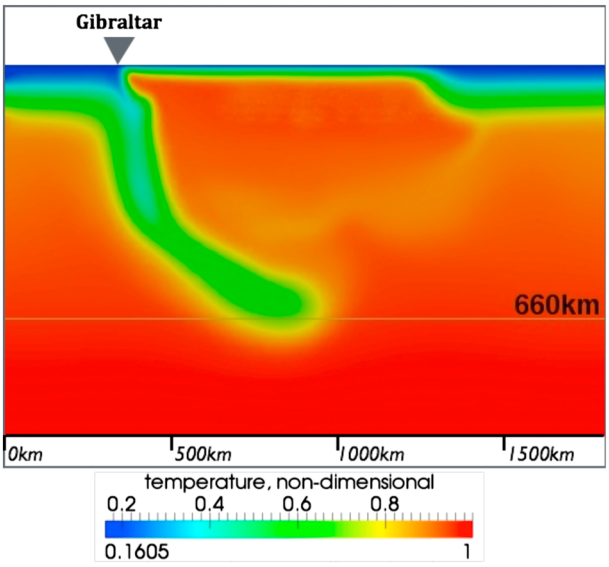

Figure 17. Cross section of the temperature field of the model S1.3-2 after 35 Ma of subduction evolution, i.e., at 0 Ma.

models S2.1-4 and S3.1-4 than for S1.3-2 even though the mantle rheology for the first two models is much stronger. The cause is the smaller initial slab buoyancy in model S1.3-2. However, after 10 My of slab evolution model S1.3-2 evolved faster as a result of gradually increasing slab buoyancy and because margin tearing evolves in the dynamically favorable geometry of a STEP [*Govers and Wortel*, 2005] where trench and margin are perpendicular. By ~10 Ma, subduction in all three models had slowed down considerably, consistent with geological constraints.

For scenario S3, by tuning rheological parameters, we managed to model the curved orientation of the trench from Gibraltar to the Iberian margin, and upper part of the slab is consistent with tomographic observations (S3.1-4). Although this resembles the geometry of model S1.3-2 around 200 km depth, deeper in the upper mantle, particularly in the transition zone, the slab is located below the African margin, which is inconsistent with tomographic models (Figure 3). The S3.1-4 slab is also thicker in horizontal cross section than S1.3-2. This deformation resulted from the stronger mantle rheology that was required for modeling rollback to the south Iberian margin. At depth, these two models become distinctly different, which primarily is due to the initial subduction configurations.

The slab shape in model S2.1-4 is completely different from the two other models. The slab was attached to the African margin through a thin "neck" under northern Morocco. The deep part of the slab in this experiment was very wide and was extending far below Iberia, which is not observed in the imaged structure of the upper mantle for this region (Figure 3).

Subduction evolution model S1.3-2 (Figures 11 and 16a) is the only one that comes close to reproducing first-order morphology and position of imaged mantle structure. It also complies with the first-order geological observation (section 3) that the subduction trench became essentially inactive around ~8 Ma. The match of predicted structure (Figure 11) to observed (Figure 3) is good in the top 300–400 km. In the deeper upper mantle, model S1.3-2 shows a more SW-NE orientation of the slab, whereas in tomography (Figure 3 and *Bezada et al.* [2013]), the orientation is more WSW-ESE. This is because the southern deep part of the slab did not roll back farther to the west. The final dipping and flattening geometry of the Gibraltar slab is presented in Figure 17 and shows a steep slab down to ~400 km depth, flattening in the transition zone. A steep Gibraltar upper mantle slab is imaged in tomography along the same W-E cross section trough the Gibraltar straight [*Gutscher et al.*, 2002; *Spakman and Wortel*, 2004; *Bezada et al.*, 2013]. The difference with the modeled slab concerns the part in the transition zone that may be too stiff to bend, or it may be too long. Slab length in this Gibraltar cross section is determined by the initial lateral stretch of lithosphere along the African margin from Gibraltar to the (dashed) oceanic weakness zone in Figure 5 (S1b) that became involved in subduction (Figure 5 (S1b)). Hence, the fit between observed and modeled slab is dependent on the initial geometry, along the African margin and in depth, of actual slab tearing in the Middle Miocene, which is unknown.

The modeled dynamic subduction evolution of model S1.3-2 provides a plausible geodynamic backbone of tectonic evolution and substantiates the tectonic evolution framework for RGB subduction as proposed by *Spakman and Wortel* [2004] that focused on slab tearing and curvature and the >180° rotation of the RGB-trench along the Betic margin. *Rosenbaum et al.* [2002], and recently *van Hinsbergen et al.* [2014] reconciled the first-order aspects of the geological evolution of the region with this geodynamic subduction framework.

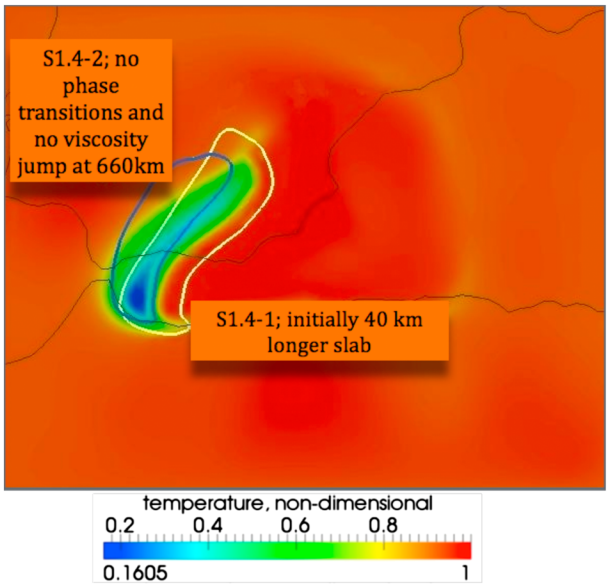

Figure 18. Comparison of models S1.3-2 (color contoured temperature plot) with a model starting from a longer initial slab (S1.4-1, yellow contour) and with a model having no phase changes and no viscosity jump (S1.4-2 blue contour). The cross section is taken after 35 Ma of subduction, i.e., at 0 Ma.

For scenario S2 we could not find a model that correlates well with the tomographic observation of slab structure of the western Mediterranean despite tuning the rheology of the mantle and margins or the initial slab length. Similarly, we failed to find such slab evolution model for S3. For scenarios S2 and S3 we conclude from our experiments that the dynamically modeled slab evolution is quite different from how subduction evolution was originally portrayed to occur in each scenario. Therefore, these proposed slab evolution scenarios cannot be considered to constitute a viable dynamic underpinning of the tectonic evolution scenarios S2 and S3.

6.2. Sensitivity of Subduction Model S1.3-2 to Variations in Initial Conditions

For our preferred model, S1.3-2, we performed several tests for the sensitivity of subduction evolution to changes in the initial model configuration (Figure 6 (S1b)).

The first test concerned the model domain size, which we could keep relatively small owing to the use of open boundaries allowing for lateral inflow and outflow [*Chertova et al.*, 2012]. We performed a test with increased lateral domain dimensions. The resulting model S1.4-3 (Figure S4 in the supporting information) confirms the findings of *Chertova et al.* [2012] that slab evolution is not strongly dependent on domain size when using open side boundary conditions, which was implemented in our models.

The second test concerned the initial amount of subduction under Baleares margin, which is constrained to ~90–150 km [*van Hinsbergen et al.*, 2014]. We ran model S1.4-1 (Table 2) with a 40 km longer slab than that used for S1.3-2. The final position of the slab is more to the east, is less rotated, and the slab is somewhat thicker (Figure 18). This is all caused by earlier interaction of the slab with the more viscous transition zone and 660 boundary resisting further sinking and westward rollback.

With the next model S1.4-2 we tested the influence of the absence of phase transitions and of the viscosity jump at 660 km. The resulting slab is at the present-day position, but the trench is less rotated and the slab has a smaller N-S extent (Figure 18). Primarily, the absence of the phase transition and associated viscosity jump allows the slab to sink into the lower mantle, which also allows initiation of lithosphere tearing along the Iberian margin.

Another test concerned the dependence of subduction evolution on the initial thermal structure of the subduction channel. We prescribed sublithosphere temperature conditions into the subduction channel, which resulted in faster initiation of slab rollback (model S1.4-4). The resulting geometry of the RGB-slab for this model is shown in Figure 19 and reveals only small differences with S1.3-2. The final position at the Gibraltar Strait is the same. The major difference is a slightly longer and thicker slab in its NE edge. This resulted from the faster rollback evolution, which lowers the deforming stresses at the pivoting point for slab rotation at the transition from the Baleares to the Iberian margin.

The location of slab stalling at ~8–10 Ma may be correlated with the position at which we end a weak African margin in the Moroccan Rif region. To test this, we terminated the weak margin 50 km more to the east. The resulting shape of the slab of this model S1.4-5 is shown in Figure 20, which shows that slab rollback stalled 30 km more to the east. Hence, the transition from the weak African margin to strong Atlantic lithosphere proves to be important for the rollback evolution.

The last experiment tested for the rheological strength of thickened south Iberian margin. In model S1.4-5 the equal strength of the continental margin and oceanic lithosphere prevented early lithosphere tearing along a

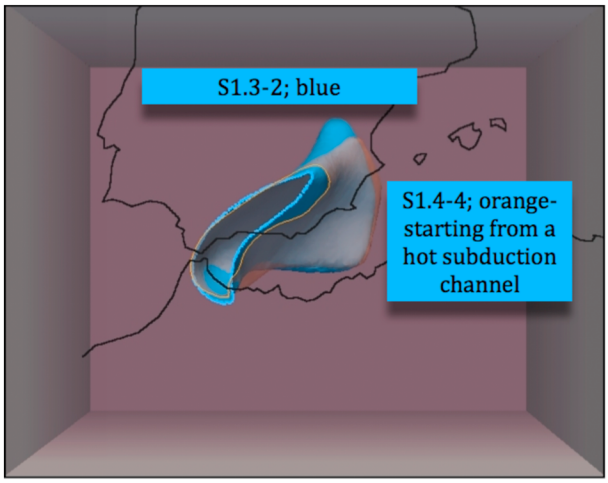

Figure 19. The present-day slab shape below 200 km for model S1.4-4 (shown in transparent orange) in comparison with model S1.3-2 (Figure 11; light blue).

thickened (Figure 5 (Sb)) Iberian margin and facilitated trench rotation. However, this model failed to reproduce possible slab breakoff under the eastern Betic since ~10 Ma, as interpreted from mantle tomography [*Spakman and Wortel*, 2004; *Bezada et al*., 2013; *Palomeras et al*., 2014]. In model S1.4-6 we used $\tau_{max} = 300$ MPa for the thickened Iberian margin. The resulting end stage of this model is shown in Figure 21 in comparison with model S1.4-4 (transparent blue), which both have the same "hot" subduction channel. The divergence in the evolution of the subduction process for these models started at ~20 Ma. Model S1.4-6 demonstrated a slightly faster rollback rate leading to a slightly more westerly position of the slab at 10–12 Ma. Interestingly, since 10–12 Ma slab breakoff developed under the eastern Betic margin. In the final stage, the Betic segment of the slab was ~200 km shorter laterally than in model S1.3-2 which improves the correlation with the imaged shallow slab structure (Figure 3).

These sensitivity tests demonstrate the robustness of the slab evolution underpinning tectonic evolution scenario S1 with respect to small changes in initial conditions.

6.3. Stress-Limited Nonlinear Rheology for Slab, Mantle, and Margins

In our modeling we used a visco-plastic rheology with a simple stress-limiting mechanism (equation (5)), which facilitated slab bending and trench retreat. The dominant parameters determining the strength of the lithosphere are γ and τ_{max} (equation (5)). This parameterization of the stress-limiting mechanism is the same as used by others [e.g,. *Schott and Schmeling*, 1998; *Enns et al*., 2005; *OzBench et al*., 2008; *Mason et al*., 2010; *Magni et al*., 2012] where γ is varied between 0.055 and 0.9 and τ_{max} between 100 and 1200 MPa. When the lower bound (0.055) is implemented for our modeling, then even with a high τ_{max} of 800 MPa, the stress-limiting rheology facilitates easy slab bending leading to fast slab steepening and detachment already after ~15 My of evolution (Figure S2 in the supporting information). Increasing the value for γ counteracts early detachment, but when it reaches 0.6–0.7 the slab becomes too stiff to bend, hampering subduction evolution. For our models we found an appropriate range for γ of 0.3–0.6 independent of the value of τ_{max}. The strength of the slab in terms of τ_{max} should be between 600 and 800 MPa. Our results suggest that slabs of age $>$ 100 Ma and subducted since the middle Cenozoic under these conditions are too strong for significant stretching. In this case, slab stretching can be ignored when comparing estimated slab length/volumes from tomography with predictions from tectonic reconstruction [e.g., *de Jonge et al*., 1994; *Spakman and Wortel*, 2004; *Spakman and Hall*, 2010]. Similar to laboratory experiments

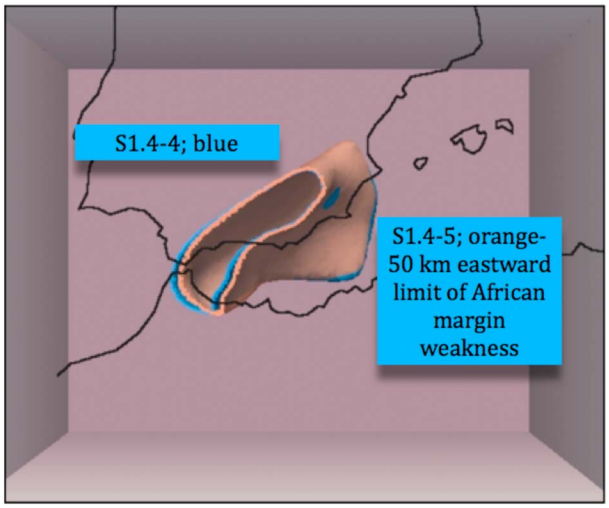

Figure 20. The present-day slab shape below 200 km for model S1.4-5 (orange color). Model S1.4-4 (Figure 19) is given for comparison in transparent light blue.

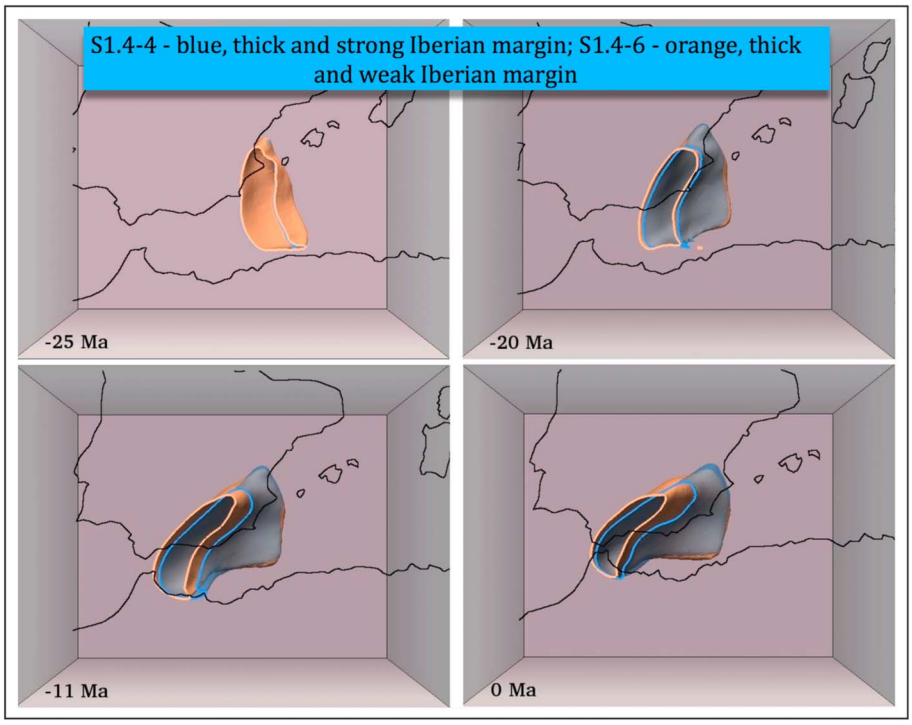

Figure 21. Evolution of the model S1.4-6 (orange contour) below 200 km. In blue transparent color model S1.4-4 (Figure 19) is shown.

[e.g., *Funiciello et al*., 2008], we observe that strong slabs can still develop very rapid slab rollback with trench speeds of up to 8 cm/yr, as in our modeling.

Our values of τ_{max} for the slab and the continental lithosphere, 600–800 MPa, are different from the values given in *Alisic et al*. [2012], who suggested a lithosphere-strength of 100 MPa from a global fit to various observables in a global instantaneous dynamic modeling. In our case, using a maximum yield stress lower than ~300 MPa invariably resulted into too weak slabs that formed holes and stretched dramatically during rollback. This led to slab morphologies such as a flat-lying slab in the transition zone under the entire region covered by the Alboran and Algerian basins, which is not observed (Figure 3 and Figure S1 in the supporting information).

In our models we do not attempt to include the complexities of continental (margin) rheology, which are still not well known (see *Burov* [2011], for a comprehensive review). We adopted the same nonlinear rheology as for the mantle and tuned overall margin strength with one parameter, τ_{max}. Tearing of continental margins is implied by all tectonic scenarios of the region and inferred from geochemical observations [*Coulon et al*., 2002; *Duggen et al*., 2004, 2005], and tomographic observations [*Spakman and Wortel*, 2004]. Another example of continental margin tearing is the recent westward propagation of the Ryukyu trench in the direction of Taiwan [*Lallemand et al*., 2001]. This indicates that continental margins are not necessarily strong when subject to a combination of laterally and vertically directed shear tractions owing to oblique plate convergence.

Our experiments required margin or slab tearing without which observed slab structure in the mantle could not be explained. For margin tearing to occur through viscous necking, we inferred from our experiments that the effective strength, as denoted by τ_{max}, should be significantly smaller (τ_{max} = 50–300 MPa) than the strength of the slab (600–800 MPa), which allowed for tear propagation along the African margin. We note that our modeling of slab tearing/detachment is less elaborate than in *Duretz et al*. [2011] and *Duretz and Gerya* [2013] who implemented Peierls creep as the plasticity mechanism and could model both necking and shearing effects for lithosphere tearing. In addition, they incorporated compositional buoyancy forcing particularly of oceanic and continental crust. Our slab tearing occurred almost always quite as shallow as we have prescribed the rheological weakness in the continental margin. The exception was model S2.1-4 (Figure 13; section 5.2).

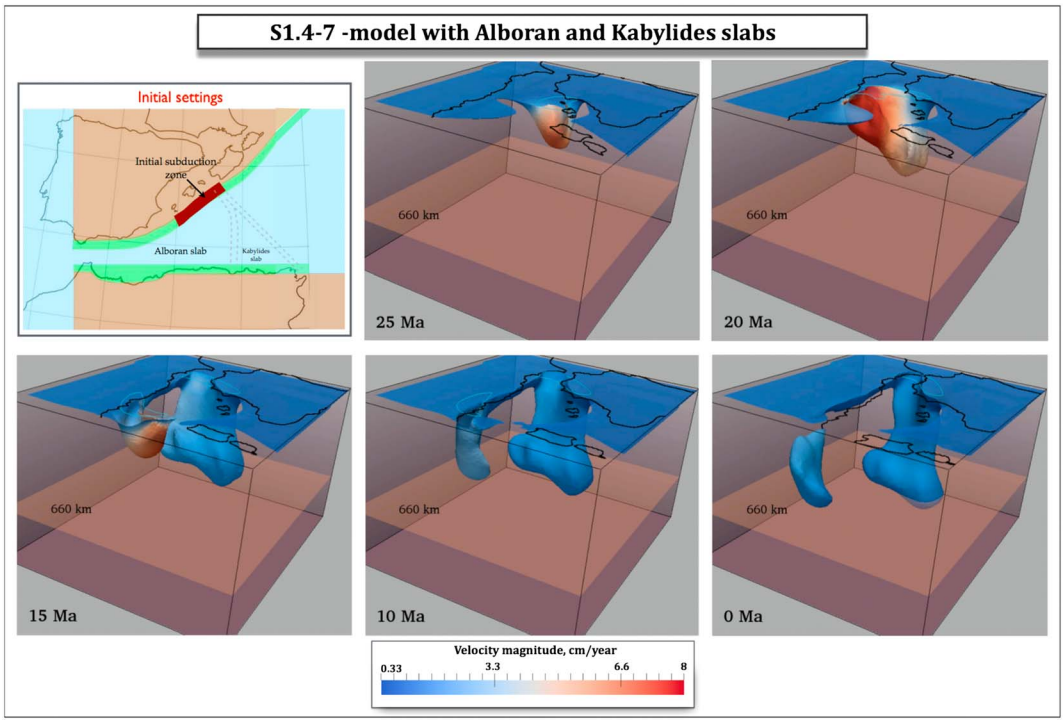

Figure 22. Model S1.4-7 that includes the evolution of the Kabylides slab. View from the NE.

The viscosity of the upper mantle depends on activation parameters for diffusion and dislocation creep (equation (5)). We have tested different values for these parameters to find an optimum for each reconstruction scenario. Rheological settings and values that led to the best-fitting slab evolution belong to the third group of experiments for tectonic scenario S1 (Table 2). For the other tectonic evolution models we attempted to optimize the fit between predicted and observed mantle structure by tuning mantle and margin rheology, but "best" values cannot be taken as useful as these models fail in producing a proper prediction of the mantle structure.

6.4. Role of the Weakness Zone at the Eastern Edge of the Oceanic Domain

The early phase of subduction in which rollback to the African margin started may depend on our implementation of the transition/weakness zone to the oceanic domain in the east, as well as on the fact that we did not model the subduction evolution of the eastern domain that ended up to form the detached Kabylides slab, and the Apennines-Calabria subduction system [e.g., *Faccenna et al*., 2004; *Spakman and Wortel*, 2004; *van Hinsbergen et al*., 2014]. Our simplification of this boundary causes a larger degree of freedom and higher flow speeds to develop and thus the modeled speed of initial subduction rollback may be higher than in reality.

To assess the influence of the eastern subduction boundary, we included (part of the) subduction of the eastern domain by constructing an initial condition that incorporates subduction of the Kabylides slab. To this end we extended the starting configuration of scenario S1 with a triangular zone of oceanic lithosphere east of the dashed weakness zone in Figure 5 (S1b). The tip of this triangular zone is at the Baleares margin while it is ~400 km wide along the east Algerian margin (see Figure 2, Scenario 1). Each long side of triangular zone constitutes a lithospheric weakness zone as in Figure 5 (S1b).

Using the same rheological settings as for model S1.3-2 (Table 2 and Figure 11), the slab evolution of this two-slab model, S1.4-7, is portrayed in Figure 22. The spatial evolution of the RGB-slab in the presence of the Kabylides slab is similar to that in model S1.3-2 (Figure 11), while the Kabylides slab evolves separately. At 10 Ma, the RGB-slab is located almost in the present-day position, however, in comparison to the S1.3-2 model (Figure 11), it is located ~50 km to the east. The predicted location of the Kabylides slab matches its (blurred) tomographic image (Figure 3). Some important differences occur in the temporal

evolution. First, the initial phase of stationary subduction of the RGB slab is now longer and takes around 8–10 My until 27–25 Ma. The RGB slab rolls back to the African margin where lithosphere tearing develops between 20 and 15 Ma. Around 15 Ma the Kabylides slab has also reached the African margin and detaches during the past 10 My. The addition of the Kabylides segment considerably improves the overall temporal evolution of slab rollback leading to a good match with the emplacement of the Kabylides on the African margin in the mid-Miocene [*Faccenna et al*., 2004; *Michard et al*., 2006; *van Hinsbergen et al*., 2014].

7. Conclusions

We set out to test, by 3-D numerical modeling, the dynamic subduction evolution of the western Mediterranean since ~35 Ma as perceived, or portrayed, in three disparate tectonic reconstruction scenarios. From each scenario we determined an initial buoyancy condition, at 35 Ma, in terms of initial subduction zone configuration from which the 3-D slab evolution evolves dynamically and self-consistently. We experimented extensively with varying the nonlinear rheology of mantle, slab, and continental margins, and by varying initial slab configurations. For each scenario, we attempted to optimize the fit between predicted slab morphology after 35 My of model evolution and that observed with seismic tomography. This leads to the following conclusions:

1. A positive match between predicted and observed slab morphology was obtained for the subduction model of tectonic scenario S1 in which initial NW-directed subduction is restricted to the Baleares margin. For scenario S2, in which initial N-NW directed subduction from Gibraltar to the Baleares is proposed, we could not find a subduction model that reasonably fits present-day observations of mantle structure. Although scenario S3 that starts from initial S-SE-directed subduction under the north-African margin may successfully explain the slab structure in the top few hundred kilometers of the mantle, it leads to a slab extending far below the African continent, which is inconsistent with tomographic constraints.
2. We conclude from many experiments that the subduction evolution as portrayed for scenario S1 can be numerically simulated to produce an end-stage slab morphology close to that observed while satisfying the temporal constraints that the slab rolled back to the north African margin in the Middle Miocene (15 Ma) and was almost in its current position in the Tortonian (10–8 Ma). The robustness of the S1-slab evolution is demonstrated by several experiments varying the settings of model S1.3-2 that is based on a strong (800 MPa) and thickened south-Iberian margin (Figure 11). In particular, model S1.4-6 (Figure 21) shows that a thickened margin with an overall strength of 300 MPa leads to slow slab tearing since the Tortonian. In model S1.4-7 (Figure 22) we included subduction of the Kabylides slab in the east and demonstrated a significant improvement of the temporal evolution constrained by rollback having reached the north-African margin by the Middle Miocene.
3. The following ranges in rheological parameters characterize our successful models: Slab strength is between 600 and 800 MPa for slab age $>$ 100 My; African continental margin strength varies between 50 and 200 MPa for STEP-tearing; the south Iberian margin was thickened prior to the Miocene by 30 km due to Africa-Iberia contraction, and its margin strength is larger than ~300 MPa; an appropriate range for γ is 0.3–0.6 independent of the value of τ_{max}; activation volumes for diffusion and dislocation creep are 4–5 $cm^3\,mol^{-1}$ and 8–9 $cm^3\,mol^{-1}$ respectively. The old slab ($>$100 Ma) under these conditions is quite strong and cannot appreciably stretch during the subduction process.
4. The dynamic slab evolution of the successful numerical models of scenario S1 comprises the following first-order geodynamic attributes that link to the tectonic/geological evolution of the region: (a) Rollback to the African margin of the RGB- and Kabylides slabs (required for Kabylides emplacement). (b) Westward tearing of the African margin, or slab, substantiating the explanation for the origin of, and westward trends in the geochemistry of margin volcanism. (c) A more or less "in place" RGB-slab at ~8–10 Ma after which geological observations show no evidence for subsequent trench activity. (d) A dominantly westward opening of the Algerian basin. (e) A clockwise rotation of the RGB-slab of $>$90° for the Gibraltar segment, and as a result of northward decreasing rollback rates amounts to $>$180° for the Betic segment, in accord with the dominant contractional direction as reconstructed for this region. (f) A steep eastward dipping slab under the Gibraltar arc and a slab geometry curving from Gibraltar to the NE under the Betic region with a torn margin under the central east Betic (model S1.4-6), as is observed with seismic tomography.

Our work constitutes a first step toward quantitative geodynamic underpinning of tectonic evolution scenario S1 and offers a viable subduction framework for further investigation of the geodynamic and geological evolution of the western Mediterranean. Our work demonstrates great potential of numerical simulation of geodynamic processes for constructing truly dynamics-based tectonic evolution models involving the deep driving processes of the mantle.

Acknowledgments
The data displayed in this paper are computed with the commercial software package SEPRAN (http://ta.twi.tudelft.nl/sepran/sepran.html). Main figures were produced using public domain software ParaView (http://www.paraview.org). We thank Pavel Doubrovine (Centre of Earth Evolution and Dynamics, University of Oslo) for providing us with time-averaged absolute plate velocities. M.V.C. acknowledges the Netherlands Organization for Scientific Research (NWO) for financial support (NWO grant 855.01.141). W.S. acknowledges the Netherlands Research Institute of Integrated Solid Earth Sciences (ISES) for the computation infrastructure used and support by the Research Council of Norway through its Centres of Excellence funding scheme, project 223272. D.J.J.v.H. was supported by ERC starting grant 306810 (SINK) and acknowledges an NWO VIDI grant. This is a contribution to the ESF EUROCORES TOPO-EUROPE, particularly subproject TOPO-4D.

References

Alisic, L., M. Gurnis, G. Stadler, C. Burstedde, and O. Ghattas (2012), Multi-scale dynamics and rheology of mantle flow with plates, *J. Geophys. Res.*, *117*, B10402, doi:10.1029/2012JB009234.

Alpert, L. A., M. S. Miller, T. W. Becker, and A. Allam (2013), Structure beneath the Alboran from geodynamic flow models and seismic anisotropy, *J. Geophys. Res. Solid Earth*, *118*, 4265–4277, doi:10.1002/jgrb.50309.

Amaru, M. L. (2007), Global travel time tomography with 3-D reference models, PhD thesis, Utrecht Univ., Utrecht, Netherlands.

Ammar, A., A. Mauffret, C. Gorini, and H. Jabour (2007), The tectonic structure of the Alboran Margin of Morocco, *Rev. Soc. Geol. Esp.*, *20*(3–4), 247–271.

Andrews, E. R., and M. I. Billen (2009), Rheologic controls on the dynamics of slab detachment, *Tectonophysics*, *464*, 60–69, doi:10.1016/j.tecto.2007.09.004.

Becker, T. W., C. Faccenna, R. J. O'Connell, and D. Giardini (1999), The development of slabs in the upper mantle: Insights from numerical and laboratory experiments, *J. Geophys. Res.*, *104*, 15,207–15,226, doi:10.1029/1999JB900140.

Bezada, M. J., E. D. Humphreys, D. R. Toomey, M. Harnafi, J. M. Davila, and J. Gallart (2013), Evidence for slab rollback in westernmost Mediterranean from improved upper mantle imaging, Spain, *Earth Planet. Sci. Lett.*, *368*, 51–60, doi:10.1016/j.epsl.2013.02.024.

Bijwaard, H., and W. Spakman (2000), Non-linear global P-wave tomography by iterated linearized inversion, *Geophys. J. Int.*, *141*, 71–82.

Bijwaard, H., W. Spakman, and E. R. Engdahl (1998), Closing the gap between regional and global travel time tomography, *J. Geophys. Res.*, *103*, 30,055–30,078, doi:10.1029/98JB02467.

Billi, A., C. Faccenna, O. Bellier, L. Minelli, G. Neri, C. Piromallo, D. Presti, D. Scrocca, and E. Serpelloni (2011), Recent tectonic reorganization of the Nubia-Eurasia convergent boundary heading for the closure of the western Mediterranean, *Bull. Soc. Geol. Fr.*, *182*, 279–303.

Blanco, M. J., and W. Spakman (1993), The P wave velocity structure of the mantle below the Iberian Peninsula: Evidence for subducted lithosphere below southern Spain, *Tectonophysics*, *221*, 13–34.

Burov, E. B. (2011), Rheology and strength of the lithosphere, *Mar. Pet. Geol.*, *28*(8), 1402–1443.

Calvert, A., E. Sandvol, D. Seber, M. Barazangi, S. Roecker, T. Mourabit, F. Vidal, G. Alguacil, and N. Jabour (2000), Geodynamic evolution of the lithosphere and upper mantle beneath the Alboran region of the western Mediterranean: Constraints from travel time tomography, *J. Geophys. Res.*, *105*, 10,871–10,898, doi:10.1029/2000JB900024.

Capitanio, F., and A. Replumaz (2013), Subduction and slab breakoff controls on Asian indentation tectonics and Himalayan western syntaxis formation, *Geochem. Geophys. Geosyst.*, *14*, 3515–3531, doi:10.1002/ggge.20171.

Carminati, E., M. Lustrino, and C. Doglioni (2012), Geodynamic evolution of the central and western Mediterranean: Tectonics vs. igneous petrology constraints, *Tectonophysics*, *579*, 173–192, doi:10.1016/j.tecto.2012.01.026.

Chalouan, A., A. El Mrihi, K. El Kadiri, A. Bahmad, F. Salhi, and R. Hlila (2006), Mauretanian flysch nappe in the northwestern Rif Cordillera (Morocco): Deformation chronology and evidence for a complex nappe emplacement, in *Tectonics of the Western Mediterranean and North Africa*, Special Publications, vol. 262, edited by G. Moratti and A. Chalouan, pp. 161–175, Geological Society, London, doi:10.1144/GSL.SP.2006.262.01.10.

Chertova, M., T. Geenen, A. P. van den Berg, and W. Spakman (2012), Using open sidewalls for modelling self-consistent lithosphere subduction dynamics, *Solid Earth Discuss.*, *4*, 707–744, doi:10.5194/se-3-313-2012.

Christensen, U. R., and D. A. Yuen (1984), The interaction of a subducting lithosphere slab with a chemical or phase boundary, *J. Geophys. Res.*, *89*, 4389–4402, doi:10.1029/JB089iB06p04389.

Čížková, H., J. van Hunen, A. P. van den Berg, and N. J. Vlaar (2002), The influence of rheological weakening and yield stress on the interaction of slabs with the 670-km discontinuity, *Earth Planet. Sci. Lett.*, *199*, 447–457.

Čížková, H., J. van Hunen, and A. P. van den Berg (2007), Stress distribution within subducting slabs and their deformation in the transition zone, *Phys. Earth Planet. Inter.*, *161*, 202–214.

Čížková, H., A. P. van den Berg, W. Spakman, and C. Matyska (2012), The viscosity of Earth's lower mantle inferred from sinking speed of subducted lithosphere, *Phys. Earth Planet. Inter.*, *200–201*, 56–62, doi:10.1016/j.pepi.2012.02.010.

Coulon, C., M. Megartsi, S. Fourcade, R. C. Maury, H. Bellon, A. Louni-Hacini, J. Cotten, A. Coutelle, and D. Hermitte (2002), Post-collisional transition from calc-alkaline to alkaline volcanism during the Neogene in Oranie (Algeria): Magmatic expression of a slab breakoff, *Lithos*, *62*(3–4), 87–110, doi:10.1016/S0024-4937(02)00109-3.

Crespo-Blanc, A., and J. Campos (2001), Structure and kinematics of the South Iberian paleomargin and its relationship with the Flysch Trough units: Extensional tectonics within the Gibraltar Arc fold-and-thrust belt (western Betics), *J. Struct. Geol.*, *23*(10), 1615–1630, doi:10.1016/S0191-8141(01)00012-8.

de Jonge, M. R., M. J. R. Wortel, and W. Spakman (1994), Regional scale tectonic evolution and the seismic velocity structure of the lithosphere and upper mantle: The Mediterranean region, *J. Geophys. Res.*, *99*, 12,091–12,108, doi:10.1029/94JB00648.

Dercourt, J., et al. (1986), Geological evolution of the Tethys belt from the Atlantic to the Pamir since the Lias, *Tectonophysics*, *123*, 241–315.

Díaz, J., and J. Gallart (2014), Seismic anisotropy from the Variscan core of Iberia to the Western African Craton: New constrains on upper mantle flow at regional scales, *Earth Planet. Sci. Lett.*, *394*, 48–57.

Diaz, J., J. Gallart, A. Villaseñor, F. Mancilla, A. Pazos, D. Córdoba, J. A. Pulgar, P. Ibarra, and M. Harnafi (2010), Mantle dynamics beneath the Gibraltar Arc (western Mediterranean) from shear-wave splitting measurements on a dense seismic array, *Geophys. Res. Lett.*, *37*, L18304, doi:10.1029/2010GL044201.

Doubrovine, P. V., B. Steinberger, and T. H. Torsvik (2012), Absolute plate motions in a reference frame defined by moving hotspots in the Pacific, Atlantic and Indian oceans, *J. Geophys. Res.*, *117*, B09101, doi:10.1029/2011JB009072.

Duggen, S., K. Hoernle, P. van den Bogaard, and C. Harris (2004), Magmatic evolution of the Alboran region: The role of subduction in forming the western Mediterranean and causing the Messinian salinity crisis, *Earth Planet. Sci. Lett.*, *218*, 91–108, doi:10.1016/S0012-821X(03)00632-0.

Duggen, S., K. Hoernle, P. van den Bogaard, and D. Garbe-Schönberg (2005), Post-collisional transition from subduction-to intraplate-type magmatism in the westernmost Mediterranean: Evidence for continental-edge delamination of subcontinental lithosphere, *J. Petrol.*, *46*(6), 1155–1201, doi:10.1093/petrology/egi013.

Duretz, T., and T. V. Gerya (2013), Slab detachment during continental collision: Influence of crustal rheology and interaction with lithospheric delamination, *Tectonophysics*, *602*, 124–140, doi:10.1016/j.tecto.2012.12.024.

Duretz, T., T. V. Gerya, and D. A. May (2011), Numerical modeling of spontaneous slab breakoff and subsequent topographic response, *Tectonophysics*, *502*, 244–256, doi:10.1016/j.tecto.2010.05.024.

Enns, A., T. W. Becker, and H. Schmeling (2005), The dynamics of subduction and trench migration for viscosity stratification, *Geophys. J. Int.*, *160*, 761–885.

Faccenna, C., T. W. Becker, F. Pio Lucente, L. Jolivet, and F. Rossetti (2001a), History of subduction and back-arc extension in the Central Mediterranean, *Geophys. J. Int.*, *145*, 809–820, doi:10.1046/j.0956-540x.2001.01435.x.

Faccenna, C., F. Funiciello, D. Giardini, and F. Pio Lucente (2001b), Episodic back-arc extension during restricted mantle convection in the Central Mediterranean, *Earth Planet. Sci. Lett.*, *187*, 105–116, doi:10.1016/S0012-821X(01)00280-1.

Faccenna, C., C. Piromallo, A. Crespo-Blanc, L. Jolivet, and F. Rossetti (2004), Lateral slab deformation and the origin of the western Mediterranean arcs, *Tectonics*, *23*, TC1012, doi:10.1029/2002TC001488.

Frizon De Lamotte, D., P. Leturmy, Y. Missenard, and S. Khomsi (2009), Mesozoic and Cenozoic vertical movements in the Atlas system (Algeria, Morocco, Tunisia): An overview, *Tectonophysics*, *475*, 9–28.

Funiciello, F., C. Faccenna, A. Heuret, S. Lallemand, E. Di Giuseppe, and T. W. Becker (2008), Trench migration, net rotation and slab-mantle coupling, *Earth Planet. Sci. Lett.*, *271*, 233–240.

Garel, F., S. Goes, D. R. Davies, J. H. Davies, S. C. Kramer, and C. R. Wilson (2014), Interaction of subducted slabs with the mantle transition-zone: A regime diagram from 2-D thermo-mechanical models with a mobile trench and an overriding plate, *Geochem. Geophys. Geosyst.*, *15*, 1739–1765, doi:10.1002/2014GC005257.

Gerya, T. V., D. A. Yuen, and W. V. Maresch (2004), Thermomechanical modelling of slab detachment, *Earth Planet. Sci. Lett.*, *226*, 101–116, doi:10.1016/j.epsl.2004.07.022.

Govers, R., and M. J. R. Wortel (2005), Lithosphere tearing at STEP faults: Response to edges of subduction zones, *Earth Planet. Sci. Lett.*, *236*, 505–523.

Gueguen, E., C. Doglioni, and M. Fernandez (1998), On the post-25 Ma geodynamic evolution of the western Mediterranean, *Tectonophysics*, *298*(1–3), 259–269, doi:10.1016/S0040-1951(98)00189-9.

Gutscher, M. A., J. Malod, J. P. Rehault, I. Contrucci, F. Klingelhoefer, L. Mendes-Victor, and W. Spakman (2002), Evidence for active subduction beneath Gibraltar, *Geology*, *30*, 1071–1074.

Gutscher, M. A., et al. (2012), The Gibraltar subduction: A decade of new geophysical data, *Tectonophysics*, *574–575*, 72–91, doi:10.1016/j.tecto.2012.08.038.

Handy, M. R., S. M. Schmid, R. Bousquet, E. Kissling, and D. Bernoulli (2010), Reconciling plate-tectonic reconstructions of Alpine Tethys with the geological–geophysical record of spreading and subduction in the Alps, *Earth Sci. Rev.*, *102*(3–4), 121–158, doi:10.1016/j.earscirev.2010.06.002.

Iribarren, L., J. Vergés, J. Camurri, J. Fullea, and M. Fernandez (2007), The structure of the Atlantic-Mediterranean transition zone from the Alboran Sea to the Horseshoe abyssal plain (Iberia-Africa plate boundary), *Mar. Geol.*, *243*, 97–119.

Ismail-Zadeh, A., S. Honda, and I. Tsepelev (2012), Linking mantle upwelling with the lithosphere decent and the Japan Sea evolution: A hypothesis, *Sci. Rep.*, *3*, Article 1137, doi:10.1038/srep01137.

Jolivet, L., and C. Faccenna (2000), Mediterranean extension and the Africa-Eurasia collision, *Tectonics*, *19*, 1095–1106, doi:10.1029/2000TC900018.

Jolivet, L., C. Faccenna, and C. Piromallo (2009), From mantle to crust: Stretching the Mediterranean, *Earth Planet. Sci. Lett.*, *285*, 198–209, doi:10.1016/j.epsl.2009.06.017.

Karato, S., M. Riedel, and D. A. Yuen (2001), Rheological structure and deformation of subducted slabs in mantle transition zone: Implications for mantle circulation and deep earthquakes, *Phys. Earth Planet. Inter.*, *127*, 83–108.

Kennett, B. L. N., E. R. Engdahl, and R. Buland (1995), Constraints on seismic velocities in the earth from travel-times, *Geophys. J. Int.*, *122*(1), 108–124.

Koulali, A., D. Quazar, A. Tahayt, R. W. King, P. Vernant, R. E. Reilinger, S. McClusky, T. Mourabit, J. M. Davila, and N. Amraoui (2011), New GPS constraints on active deformation along the Africa-Iberia plate boundary, *Earth Planet. Sci. Lett.*, *308*, 211–217, doi:10.1016/j.epsl.2011.05.048.

Lallemand, S., Y. Font, H. Bijwaard, and H. Kao (2001), New insights on 3-D plates interaction near Taiwan from tomography and tectonic implications, *Tectonophysics*, *335*, 229–253.

Liu, L., and M. Gurnis (2008), Simultaneous inversion of mantle properties and initial conditions using an adjoint of mantle convection, *J. Geophys. Res.*, *113*, B08405, doi:10.1029/2008JB005594.

Lonergan, L., and N. White (1997), Origin of the Betic-Rif mountain belt, *Tectonics*, *16*, 504–522, doi:10.1029/96TC03937.

Magni, V., J. van Hunen, F. Funiciello, and C. Faccenna (2012), Numerical models of slab migration in continental collision zones, *Solid Earth*, *3*, 293–306, doi:10.5194/se-3-293-2012.

Mason, W. G., L. Moresi, P. G. Betts, and M. S. Miller (2010), Three-dimensional numerical models of the influence of a buoyant oceanic plateau on subduction zones, *Tectonophysics*, *483*(1–2), 71–79, doi:10.1016/j.tecto.2009.08.021.

Mauffret, A., D. Frizon de Lamotte, S. Lallemant, C. Gorini, and A. Maillard (2004), E-W opening of the Algerian Basin (Western Mediterranean), *Terra Nova*, *16*(5), 257–264, doi:10.1111/j.1365-3121.2004.00559.x.

Melialdea, T., R. Vegas, L. Somoza, T. Vazquez, A. Maldonado, V. Diaz-del-Rio, A. Maestro, D. Cordoba, and M. C. Fernandez-Puga (2004), Structure and evolution of the "Olistostrome" complex of the Gibraltar Arc in the Gulf of Cadiz (eastern central Atlantic): Evidence from two long seismic cross-sections, *Mar. Geol.*, *209*, 173–198.

Michard, A., F. Negro, O. Saddiqi, M. L. Bouybaouene, A. Chalouan, R. Montigny, and B. Goffe (2006), Pressure-temperature-time constraints on the Maghrebide mountain building: Evidence from the Rif-Betic transect (Morocco, Spain), Algerian correlations, and geodynamic implications, *C. R. Geosci.*, *338*, 92–114, doi:10.1016/j.crte.2005.11.011.

OzBench, M., et al. (2008), A model comparison study of large-scale mantle-lithosphere dynamics driven by subduction, *Phys. Earth Planet. Inter.*, *171*, 224–234.

Palomeras, I., S. Thurner, A. Levander, K. Liu, A. Villasenor, R. Carbonell, and M. Harnafi (2014), Finite-frequency Rayleigh wave tomography of the western Mediterranean: Mapping its lithospheric structure, *Geochem. Geophys. Geosyst.*, *15*, 140–160, doi:10.1002/2013GC004861.

Piromallo, C., and A. Morelli (2003), *P* wave tomography of the mantle under the Alpine-Mediterranean area, *J. Geophys. Res.*, *108*(B2), 2065, doi:10.1029/2002JB001757.

Rosenbaum, G., G. S. Lister, and C. Duboz (2002), Reconstruction of the tectonic evolution of the western Mediterranean since the Oligocene, *J. Virtual Explor.*, *8*, 107–130.

Royden, L. H. (1993), Evolution of retreating subduction boundaries formed during continental collision, *Tectonics*, *12*, 629–638, doi:10.1029/92TC02641.

Schellart, W. P., and L. Moresi (2013), A new driving mechanism for backarc extension and backarc shortening through slab sinking induced toroidal and poloidal mantle flow: Results from dynamic subduction models with an overriding plate, *J. Geophys. Res. Solid Earth*, *118*, 3221–3248, doi:10.1002/jgrb.50173.

Schettino, A., and E. Turco (2006), Plate kinematics of the Western Mediterranean region during the Oligocene and Early Miocene, *Geophys. J. Int.*, *166*(3), 1398–1423, doi:10.1111/j.1365-246X.2006.02997.x.

Schott, B., and H. Schmeling (1998), Delamination and detachment of lithospheric roots, *Tectonophysics*, *296*, 225–247.

Spakman, W. (1986), Subduction beneath Eurasia in connection with the Mesozoic Tethys, *Geol. Mijnbouw*, *65*, 145–153.

Spakman, W., and R. Hall (2010), Surface deformation and slab-mantle interaction during Banda arc subduction rollback, *Nat. Geosci.*, *3*, 562–566, doi:10.1038/ngeo917.

Spakman, W., and M. J. R. Wortel (2004), A tomographic view on western Mediterranean geodynamics, in *The TRANSMED Atlas-The Mediterranean Region From Crust to Mantle*, edited by P. Ziegler, pp. 31–52, Springer, Berlin.

Spasojević, S., L. Liu, and M. Gurnis (2009), Adjoint models of mantle convection with seismic, plate motion and stratigraphic constraints: North America since the Late Cretaceous, *Geochem. Geophys. Geosyst.*, *10*, Q05W02, doi:10.1029/2008GC002345.

Stegman, D. R., W. P. Schellart, and J. Freeman (2010), Competing influence of plate width and far-field boundary conditions on trench migration and morphology of subducted slabs in the upper mantle, *Tectonophysics*, *483*, 46–57.

Torsvik, T. H., et al. (2012), Phanerozoic polar wander, paleogeography and dynamics, *Earth Sci. Rev.*, *114*, 325–368.

van Hinsbergen, D. J. J., R. L. M. Vissers, and W. Spakman (2014), Origin and consequences of western Mediterranean subduction, rollback, and slab segmentation, *Tectonics*, *33*, 393–419, doi:10.1002/tect.20125.

van Hunen, J. (2001), Shallow and buoyant lithospheric subduction: Causes and implications from thermo-chemical numerical modeling, PhD thesis, Utrecht Univ., Utrecht, Netherlands.

van Hunen, J., and M. B. Allen (2011), Continental collision and slab break-off: A comparison of 3-D numerical models with observations, *Earth Planet. Sci. Lett.*, *302*(1–2), 27–37, doi:10.1016/j.epsl.2010.11.035.

Vergés, J., and M. Fernàndez (2012), Tethys–Atlantic interaction along the Iberia–Africa plate boundary: The Betic–Rif orogenic system, *Tectonophysics*, *579*, 144–172, doi:10.1016/j.tecto.2012.08.032.

Vernant, P., A. Fadil, T. Mourabit, D. Quazar, A. Koulali, J. M. Davila, J. Garate, S. McClusky, and R. Reilinger (2010), Geodetic constraints on active tectonics of the Western Mediterranean: Implications for the kinematics and dynamics of the Nubia-Eurasia plate boundary zone, *J. Geodyn.*, *49*, 123–129, doi:10.1016/j.jog.2009.10.007.

Vissers, R. L. M., and P. T. Meijer (2012), Iberian plate kinematics and Alpine collision in the Pyrenees, *Earth Sci. Rev.*, *114*(1–2), 61–83, doi:10.1016/j.earscirev.2012.05.001.

Vissers, R. L. M., D. J. J. van Hinsbergen, and P. T. Meijer (2013), Kinematics of Jurassic ultra-slow spreading in the Piemonte Ligurian ocean, *Earth Planet. Sci. Lett.*, *380*, 138–150, doi:10.1016/j.epsl.2013.08.033.

Wortel, M. J. R., and W. Spakman (2000), Subduction and slab detachment in the Mediterranean-Carpathian region, *Science*, *290*, doi:10.1126/science.290.5498.1910.